

# IISc Theses Abstracts

## Contents

Genomic organization and expression of Belladonna mottle virus-Iowa (renamed Physalis mottle virus)	A. N. K. Jacob	433
Studies on tRNAs and tRNA genes in cucumber ( <i>Cucumis sativus</i> ) chloroplasts	Shailaja Hande	436
Structure-function relationship of winged bean ( <i>Psophocarpus tetragonolobus</i> ) basic agglutinin (WBA I): Carbohydrate binding, domain structure and amino acid sequence analyses	Kamal Deep Puri	438
Molecular modelling studies on wheat germ agglutinin-saccharide interactions	S. Mohan	440
Studies on the synthesis, structure and reactivity of amino and halo silanes	K. N. Radhamani	442
Infrared and Raman spectroscopic investigations of phase transitions in complex solids	Vijay Varma	444
Algorithms to test and implement fault tolerance in self-routing permutation networks	S. Ravi Shankar	446
Analysis of some smoothing techniques with application to narrow-band/broadband beamforming and DOA estimation	K. C. Indukumar	448
Design and performance study of a media access control protocol for wireless LANs	A. Chockalingam	449
Reliability and performability analysis of distributed memory multicomputers	Samir Mahmoud Koriem	454
Determining and connecting all the extrema of a function over a compact manifold	H. Shashikala	457
Studies in learning and representation in connectionist networks	S. H. Srinivasan	461
A study of partial discharge characteristics of critical zones in an insulation system of EHV transformer	K. Siddappa Naidu	464
Estimation of aircraft aerodynamic derivatives accounting for measurement and process noise by EKF through adaptive filter tuning	Moses Osmond Gemson	467
A new approach for the numerical solution of constrained mechanical systems	Rachuri Sudarsan	469
Transonic flow of a real fluid and some problems using a new theory of shock dynamics	D. Chandrasekar	474
Optimum design of composite laminates for buckling, vibration and interlaminar strength by ranking	M. Kumar	475
Analysis of buffering for a shared medium fast packet switch	B. K. Jayaram	477
Laser patterning and automated loss measurements for integrated optics	Mahadev Gurunath Lad	479
Design of induction heaters	Kamalesh Chatterjee	482



# IISc THESES ABSTRACTS

Thesis Abstract (Ph. D.)

**Genomic organization and expression of belladonna mottle virus IOWA (renamed *Physalis mottle virus*)** by A. N. K. Jacob

Research supervisors: N. Appaji Rao and H. S. Savithri

Department: Biochemistry

## 1. Introduction

Plant viral genomes generally code for a limited number of proteins which are vital to their survival. These proteins with the exception of structural proteins usually appear transiently during the infection cycle. A limited amount of information is available on their structure and function. In recent years, the use of recombinant DNA technology has enabled the study of some of these proteins. Understanding the genomic sequence and organization is an important initial step in these studies. In the present study, Belladonna mottle virus-IOWA (BDMV-I), a tymovirus which infects Solanaceae plants was used as a model system to study the organization and expression of plant RNA viral genomes<sup>1</sup>.

The smaller size of the genome and the earlier work in this laboratory prompted the selection of BDMV(I) for the study of its genomic organization and expression. The objectives of this study were: (i) to elucidate the strategies employed by BDMV(I) to express its genomic RNA into the CP and non-structural proteins; (ii) to determine the nucleotide sequence at the 3' region of the genomic RNA; (iii) analyze the sequence information for the presence of ORFs and possible regulatory signals; (iv) to compare the 3' terminal genomic sequence of BDMV(I) with those of other tymoviruses in order to discern evolutionary relationships; and (v) to understand the role of the 3' untranslated region of the genome in viral replication.

## 2. Materials and methods

The following methods were used in this study: (i) isolation of BDMV(I) from infected *N. glutinosa* plants<sup>2</sup>, (ii) procedures for *in vitro* translation<sup>3</sup> (3), (iii) preparation of a cDNA library of BDMV(I) in pUC18 and using the library to screen for clones generated from the 3' terminal region<sup>4</sup>, (iv) sequencing of the clones by direct plasmid sequencing<sup>5</sup>, (v) analysis of the sequence data generated in this study using GCG software<sup>6</sup>, (vi) aminoacylation of BDMV(I) RNA and (vii) partial purification of the replicase<sup>7</sup> and its interaction with a transcript derived from a clone corresponding to the 3' terminal region of the genomic RNA by gel retardation assays<sup>8</sup>.

## 3. Results and discussion

### 3.1. Isolation and characterization of the viral RNA

The genome of BDMV(I) consists of a positive-sense RNA molecule which is encapsidated in an icosahedral (T = 3) protein capsid of 180 identical subunits (20,000 Da). The virus was purified from infected leaves of *Nicotiana glutinosa* using standard procedures. The purified virus preparation contained two kinds of particles, in tact virion and 'empty' capsids, which could be visualized on electron microscope. These two types of particles were separated by sucrose density gradient centrifugation into two fractions, a lighter top fraction (T) which consisted essentially of empty capsids and a denser bottom fraction (B) which comprised mostly of in tact virions. Both the T- and B-fractions were shown to contain RNA. Analysis of the RNAs on formaldehyde-agarose gel showed the B-fraction to contain genomic RNA ( $2 \times 10^6$  Da), while T-fraction contained several RNA species ranging from  $0.2 \times 10^6$  to  $2 \times 10^6$  M<sub>r</sub>.

### 3.2. *In vitro* translation of BDMV (I) RNA

The strategies employed for the expression of the genomic RNA of BDMV (I) was studied by *in vitro* translation of the RNA in rabbit reticulocyte lysate system. Three proteins of M<sub>r</sub> 210, 150 and 78 K were detected as the major translation products of the B-RNA. The time course of translation of the B-component RNA indicated that the 150 K protein could arise from the processing of the 210 K polyprotein. The 70 K protein could also arise from the translation of an overlapping ORF, although the presence of such an ORF was not obvious from the partial 3' sequences obtained in the present study.

The translation of the T-component RNA of BDMV(I) yielded several products one of which reacted with the specific polyclonal antiserum raised against the CP, indicating the presence of CP mRNA. The translation of the T-component RNA isolated from infected capsicum leaves also showed the presence of the CP mRNA. These results indicated that the subgenomic mRNA for CP was preferentially encapsidated in the T-component of BDMV(I).

A model to explain the possible mechanisms for the expression of BDMV(I) genome was suggested<sup>9</sup>. The salient features of this model are that the BDMV(I) genomic RNA is translated into a polyprotein which is further processed to yield two products one of which could be the putative replicase. The CP is expressed *via* a subgenomic mRNA. In general, tymoviruses seem to follow common strategies of gene expression, such as polyprotein processing, use of subgenomic RNAs and overlapping reading frames.

### 3.3. Generation of cDNA clone sequencing and analysis of the 3' terminal 1.25 kb region of BDMV(I) RNA

In order to study the genome in greater detail, a cDNA library of BDMV(I) was constructed in the plasmid, pUC 18. Positive clones representing the 3' terminal regions of the genomic RNA were identified by colony hybridization using the first strand cDNA and/or end-labeled T-RNA as probes. Clones with progressively increasing insert size (0.2–2.0 kb) were selected to form an overlapping set which was then sequenced by direct plasmid sequencing method. A contiguous sequence of 1255 nt corresponding to the 3' region of the genome was obtained and assembled.

The sequence of 1255 nt at the 3' end was analyzed using GCG software package to identify the presence of ORFs, non-coding regions and regions which could form secondary structures. This analysis revealed a complete ORF corresponding to the CP and a partial ORF for the C-terminal 178 residues of the RP. Downstream to the CP gene a non-coding region was identified which could be folded into a stem-loop structure. The sequence corresponding to C-terminal 178 residues of RP was compared with similar regions in other tymoviruses. This comparison revealed a high degree of sequence homology among the RP sequences of tymoviruses. Within the coding region of RP, upstream of the CP ORF, a highly conserved stretch of 17 nucleotides (Tymobox)<sup>10</sup>, observed in other tymoviruses, was also identified in BDMV(I). The functional importance of this region is discussed.

The deduced amino acid sequence of the CP was identical to that obtained by direct protein sequencing carried out earlier in our laboratory, except for the presence of an extra dipeptide at position 111–112 in the latter<sup>11</sup>. A comparison of the CP sequences of 9 tymoviruses including BDMV(I) revealed that the overall homology was less than that observed when the Rps were compared. Another unusual feature noticed in this comparison was the invariant presence of glycines at several positions in the sequence, although this was not an abundant amino acid in the protein. These glycines might be present at interstrand regions and hence important for maintaining the tertiary structure.

It was observed that BDMV(I) CP lacked a basic amino terminal arm which was invoked for stabilizing the protein RNA interactions in the case of several other viruses<sup>12</sup>. Polyamines which altered the spectral properties of the RNA probably replaced the function of the basic amino terminal arm. An expressing clone of BDMV(I) was identified by immunoscreening, Western blotting and IPTG induction experiments. Sequencing this clone showed that the protein was truncated at the N-terminus by 21 amino acids and was inframe with lac Z gene of the vector. This truncated protein could be used in future for establishing the role of the N-terminal region in the assembly of BDMV(I).

The analysis of the 3' terminal noncoding region showed that the terminal 80 nt could be folded into a characteristic tRNA-like structure. Within this structure, a sequence capable of forming a 'pseudoknot'<sup>13</sup> was seen as a part of the aminoacyl acceptor arm. The alignment of this region with corresponding regions of other tymoviruses revealed that the loops were better conserved than the base paired regions. One possible reason for the high degree

of conservation of the loops could be their involvement in interactions with viral/host proteins participating in viral replication.

A phylogenetic tree<sup>14</sup> to position BDMV(I) among tymoviruses was constructed based on aligned sequences of CPs and C-terminal 178 residues of RPs. The trees obtained using either CP or the RP sequences had similar topology. The trees showed that BDMV(I) was closer to EMV than BDMV(E), regarded as a related strain of the same virus. In view of this observation, it is suggested that BDMV(I) be renamed *Physalis mottle virus* (PhMV).

### 3.4. Functional importance of 3' terminal region of BDMV(I) genomic RNA

The functional importance of 3' terminal region of the genomic RNA was studied by carrying out aminoacylation experiments and the interaction of a partially purified replicase with a labeled transcript obtained from a clone containing the 3' terminal 240 nt. The aminoacylation experiments showed that the tRNA-like structure was capable of accepting valine in preference to other amino acids. The physiological significance of this structure to be acylated by valine is not yet clear.

The viral replicase was identified and solubilized from infected *N. glutinosa* leaves. The product of the replicase reaction had an  $M_r$  identical to the expected size of the genomic RNA indicating that it was capable of synthesizing full-length genomic RNA. The interaction of the replicase with a transcript corresponding to the 3' terminal portion of the genomic RNA was examined by first constructing a subclone of TA42 in pBlue script. The transcript corresponding to 3' terminal 240 nt was shown to bind to the partially purified replicase in gel mobility shift assays and to inhibit the activity of the enzyme in *in vitro* assays.

The results described in this thesis showed that BDMV(I) followed the strategy of polyprotein processing and subgenomic RNA production for the expression of its proteins. The 3' terminal genomic RNA sequence determined in this study revealed the presence of a non-coding region at the 3' end possibly involved in the regulation of replication, the CP gene, and the C-terminal 178 residues of the RP gene. A quantitative comparison of this sequence with those of other tymoviruses indicated that BDMV(I) is not a strain of BDMV(E) but a distinct tymovirus, now renamed *Physalis mottle virus*.

### References

1. SAVITHRI, H. S. AND JACOB, A. N. K. *J. Indian Inst. Sci.*, 1993, 73, 55-71.
2. SAVITHRI, H. S., MUNSHI, S. K., SURYANARAYANA, S., DIVAKAR, S. AND MURTHY, M. R. N. *J. Gen. Virol.*, 1987, 68, 1533-1542.
3. PELHAM, H. R. B. AND JACKSON, R. J. *Eur. J. Biochem.*, 1976, 67, 247-256.
4. JACOB, A. N. K., MURTHY, M. R. N. AND SAVITHRI, H. S. *Arch. Virol.*, 1992, 123, 367-377.
5. CHEN, E. Y. AND SEEBURG, P. H. *DNA*, 1985, 4, 165-170.
6. DEVEEREUX, J., HAEBERLI, P. O. AND SMITHIES, O. *Nucl. Acids Res.*, 1984, 12, 387-395.
7. HAYES, R. J. AND BUCK, K. W. *Cell*, 1990, 63, 363-368.
8. KONARSKA, M. M. AND SHARP, P. A. *Cell*, 1986, 46, 845-855.
9. JACOB, A. N. K. AND SAVITHRI, H. S. *Indian J. Biochem. Biophys.*, 1991, 28, 456-460.
10. DING, S. *et al.* *Nucl. Acids Res.*, 1990, 18, 1181-1187.
11. SURYANARAYANA, S., APPAJI RAO, N., MURTHY, M. R. N. AND SAVITHRI, H.S. *J. Biol. Chem.*, 1989, 264, 6273-6279.
12. SURYANARAYANA, S. *Structure and stability of Belladonna mottle virus*, Ph. D. Thesis, Indian Institute of Science, Bangalore, 1989.

13. PLEIJ, C. W. A. *Trends Biochem. Sci.*, 1990, 15, 143-147.  
 14. FITCH, W. M. AND MARGOLIASH, E. *Science*, 1960, 155, 279-284.

### Thesis Abstract (Ph. D.)

## Studies on tRNAs and tRNA genes in cucumber (*Cucumis sativus*) chloroplasts by Shailaja Hande

Research supervisor: G. Padmanaban

Department: Biochemistry

### 1. Introduction

Chloroplasts are semi-autonomous energy-transducing photosynthetically functional organelles found in plant cells. These organelles develop from precursors known as proplastids when exposed to light and to etioplasts when kept in dark. They contain their own DNA, RNA and all the machinery involved in replication, transcription and translation.

The objectives of the present investigation were: (1) To study the effect of light on chloroplast tRNA gene expression in cucumber (*Cucumis sativus*). (2) To purify and sequence a chloroplast tRNA<sup>Pro</sup> by post-labeling techniques to understand the unique secondary structural features. (3) Cloning, sequencing and characterization of a tRNA[tRNA<sup>Leu</sup> (CAA)] gene and to study its organization and processing.

### 2. Experimental

Plastid tRNAs were prepared from cucumber cotyledons according to the procedure of Shinozaki and Sugiura<sup>1</sup>. Aminoacylation assays and 2D-PAGE were carried out according to the procedures of Burkard *et al.*<sup>2,3</sup> tRNA sequencing was done according to the method of Stanley and Vassilenko<sup>4</sup>. Studies on tRNA processing were carried out according to the method of Poll *et al.*<sup>5</sup>.

### 3. Results and discussion

#### 3.1. Effect of light on tRNA gene expression

Light is the coordinator of several events at different stages of leaf formation and the transformation of etioplasts to chloroplasts is one such developmental event that is mediated by light. The development of photosynthetically functional chloroplasts requires the coordinated expression of both nuclear and chloroplast genes since chloroplast proteins are coded by both nuclear and chloroplast genes. Recent developments have shown that light modulates the expression of nuclear genes coding for chloroplast proteins at the level of transcription, whereas it modulates the expression of chloroplast genes by post-transcriptional, translational and post-translational events. In order to examine the role of light in the modulation of chloroplast tRNA genes the following experiments were conducted.

To study and compare tRNA population in etioplasts and chloroplasts, <sup>32</sup>P-labeled total tRNA from the two sources was fractionated by two-dimensional polyacrylamide gel electrophoresis (2D-PAGE) and subjected to autoradiography.

Comparison of the autoradiograms revealed a similar pattern in both the plastid types except for the presence of nine extra tRNA species in etioplasts. These extra tRNA species could be due to the presence of tRNA with variation in their modified nucleotide content or due to the presence of new tRNA isoacceptors.

The relative levels of specific tRNAs in chloroplasts and etioplasts were determined by aminoacylation using *E. coli* aminoacyl synthetases and tritiated amino acid. The results obtained indicated that the levels of most of the tRNAs remained more or less equal in the two plastids. However, the amino acid acceptor activity of tRNA<sup>Lys</sup>, tRNA<sup>Arg</sup> and tRNA<sup>Tyr</sup> (40, 44 and 50%, respectively) were dramatically reduced in etioplasts as compared to that in chloroplasts.

Northern analysis of specific chloroplast tRNAs, namely, tRNA<sup>Leu</sup>(CAA), tRNA<sup>Leu</sup>(UAG), tRNA<sup>Leu</sup>(UAA), tRNA<sup>Phe</sup>(GAA), tRNA<sup>Thr</sup>(GGU), tRNA<sup>Glu</sup>(UUC) and tRNA<sup>Tyr</sup>(GUA) was carried out using gene-specific probes.

The data obtained revealed that with the exception of tRNA<sup>Thr</sup>(GGU), whose levels increased in etioplasts, the relative levels of most plastid tRNAs tested did not change appreciably in the two plastid types. However, aminoacylation data revealed reduced levels of functional tRNA<sup>Tyr</sup> in etioplasts. This suggested that reduced aminoacylation of tRNA<sup>Tyr</sup> could be due to defective tRNA<sup>Tyr</sup> molecules (loss of 3'-CCA ends or undermodified tRNA<sup>Tyr</sup>).

The extra tRNA species in the 2D-gels prompted us to investigate the isoacceptor profile of certain tRNAs as well as the degree of modification in total tRNA in etioplasts and chloroplasts. Light-induced alterations in the tRNA isoacceptor profile of tRNA<sup>Leu</sup>, tRNA<sup>Phe</sup>, tRNA<sup>Val</sup> and tRNA<sup>Lys</sup> in etioplasts and chloroplasts were examined by RPC-5 column chromatography of aminoacylated tRNAs. The results indicated that there were no changes in the number of isoacceptor species for these tRNAs. However, there were significant differences in the relative levels for two of the three tRNA<sup>Leu</sup> isoacceptors and for both the isoacceptors of tRNA<sup>Val</sup>. This indicated that although light did not cause the induction of new tRNA isoaccepting species for the tRNAs tested, it modulated the expression of these tRNA genes.

Since modified nucleotide content of tRNA has an impact on the activity of tRNA, the effect of light on the modified nucleotide content of etioplast and chloroplast tRNAs was examined, by the post-labeling technique. Modified nucleotides pi<sup>6</sup>A/piO<sup>6</sup>A, pU, pm<sup>2</sup>A, pGm, pm<sup>2</sup>G, pm<sup>1</sup>G, pTm, pT, pI, pD, pm<sup>3</sup>C, pm<sup>7</sup>G, pCm and pm<sup>1</sup>A were identified in both total tRNA species. However, etioplast tRNAs were undermodified with respect to the modified nucleotides pi<sup>6</sup>/piO<sup>6</sup>A, pU, pI, pGm, pm<sup>1</sup>G, pT and pTm, while chloroplast tRNAs were undermodified with respect to pm<sup>1</sup>A and pm<sup>2</sup>A. Hence it is probable that the differences in the number of tRNA species that were observed in the 2D-gel pattern and the amino acid acceptor activity of tRNA in the two plastid types were due to the variations in the extent of tRNA modification. In conclusion, relative levels and/or amino acid acceptor activity of only some of the tRNA molecules studied were altered under conditions of etiolation. Since tRNAs play an important role in protein synthesis, limiting quantities of certain tRNA might have a regulatory role in protein synthesis. The results obtained suggested that transcriptional regulation occurs to a limited extent and that post-transcriptional events such as turn over, stability, modification and processing of tRNA probably play a major role in the control of tRNA gene expression in light-mediated changes brought about in chloroplasts.

### 3.2. Structural features of tRNA<sup>Pro</sup>

In order to study the tRNA population in cucumber chloroplasts, total chloroplast tRNA (cold tRNA mixed with <sup>32</sup>P-labeled tRNA) were fractionated by 2D-PAGE. The tRNA resolved into 37 species out of which 20 tRNA corresponding to 12 amino acids were identified by aminoacylation with *E. coli* aminoacyl-tRNA synthetases.

In order to study the structural aspects of chloroplast tRNA<sup>Pro</sup> it was purified by RPC-5 column chromatography and 2D-PAGE. The sequence of this tRNA was determined by post-labeling technique. It was 77 nucleotides in length and had all the variant and semi-invariant features found in most tRNAs. It had the anticodon UGG. The most unusual feature of this tRNA was the absence of methylated GG residues at positions 18 and 19 in the dihydrouridine loop. It had the modified nucleotides pD (positions 20), pU (positions 27, 38 and 55), pm<sup>7</sup>G (position 46), pT (position 54), and an unknown modified A residue (position 37).

### 3.3. Study of tRNA biosynthesis

To study the organization, expression and biosynthesis of tRNA genes in cucumber chloroplast, a chloroplast genomic library was constructed using the vector pUC8 and the clones were screened with 3' end labeled chloroplast total tRNAs. Six positive clones were identified and one of the clones, pCL19 carrying a DNA segment of 1.7 kb was isolated, subcloned and the sequence of the tRNA gene determined. The DNA segment contained tRNA<sup>Leu</sup>(CAA) gene. The coding region of the gene was 81 bp long and showed 99% homology with the corresponding gene from spinach, broad bean, tobacco and maize, 98% homology with pea and 90% homology with livewort. The 5' flanking region of the gene contained two sets of -10-like (TATCAT and TAGAT) and -35-like (TTCCAT and TTGTCA) bacterial promoter sequence. The 3' flanking region showed inverted repeats that could be transcription terminator signals.

Towards delineating the steps involved in the processing of the above tRNA gene, a 714 bp subfragment of clone pCL19 containing the gene was subcloned in the vector pSP64. <sup>32</sup>P-labeled precursor prepared from this subclone using SP6 RNA polymerase was incubated with pea chloroplast extract. In this study, mature tRNA was

observed in all the experiments. It was shown that endonucleases were involved in the maturation of 5' and 3' ends of this tRNA. However, the simultaneous occurrence of the intermediates 5' leader + tRNA and 3' trailer + tRNA suggested that *in vitro* there was no specific order in the processing steps.

### References

1. SHINOZAKI, K. Y. AND SUGIURA, M. *Nucl. Acids Res.*, 1982, 10, 4923.
2. BURKARD, G., GUILLEMAUT, P. AND WEIL, J. H. *Biochem. Biophys. Acta*, 1970, 224, 184.
3. BURKARD, G. *et al.* In *Methods in chloroplasts molecular biology* (Edelman, M., Hallick, R. B. and Chua, N. H., eds), p. 347, 1982, Elsevier Biomedical Press.
4. STANLEY, J. AND VASSILENKO, S. *Nature (Lond.)*, 1978, 274, 87.
5. POLL, A. M., HIBBERT, C. S., RADEBAUGH, C. A. AND HALLICK, R. B. *Pl. Mol. Biol.*, 1988, 11, 45.

### Thesis Abstract (Ph. D.)

**Structure–function relationship of winged bean (*Psophocarpus tetragonolobus*) basic agglutinin (WBA I): Carbohydrate binding, domain structure and amino acid sequence analyses** by Kamal Deep Puri  
 Research supervisor: Avadhesh Surolia  
 Department: Molecular Biophysics Unit

#### 1. Introduction

Lectins are multivalent carbohydrate-binding proteins or glycoproteins of non-immune origin which agglutinate cells and/or precipitate glyco-conjugates. Although first discovered in 1888, lectins attracted only limited attention until the early 1960s. The application of lectins in studying the biology of carbohydrates and in biological research started to gain momentum only in the late 1960s. This was mainly due to two discoveries made in the early 1960s, firstly, that certain lectins possess the ability to stimulate lymphocytes to undergo mitosis and secondly that certain lectins preferentially agglutinate malignant cells as compared to their normal counterparts. Numerous studies followed that gradually led to the widespread use of lectins in biological and medical research. As all the activities of lectins are manifestations of their sugar specificities, and as they provide prototype model systems for the interactions that occur at cell surfaces as well as protein–sugar interactions, and in order to use them as sensitive cell-surface probes, a detailed elucidation of their carbohydrate specificity is imperative<sup>1</sup>.

#### 2. Experimental

##### 2.1. Thermodynamic studies on the binding of winged bean basic agglutinin (WBA I) with various blood group A- and B-reactive sugars

Carbohydrate-binding specificity and the forces involved in the stabilization of WBA I-ligand complex were determined using N-dansylgalactosamine as the reporting fluorophore. The  $\alpha$ -linked disaccharides of Gal and GalNAc are considerably better ligands than their  $\beta$ -linked counterparts. Combining site of WBA I is extended and encompasses all the residues of blood group A-reactive trisaccharide (GalNAc $\alpha$ 3Gal $\beta$ 4Glc)<sup>2</sup>. Terminal  $\alpha$ 1-3-linked GAINAC is indispensable. The presence of an acetamido group at C-2 position of GAINAC increases the affinity by about 5-fold over that of a hydroxyl group. Though both the fucose residues of A-pentasaccharide (GalNAc $\alpha$ (Fuc $\alpha$ 2) 3Gal $\beta$ (Fuc $\alpha$ 3) 4Glc) do not directly interact with the combining site they thermodynamically favour the interaction of the binding epitope (GalNAc $\alpha$ 3Gal $\beta$ 4Glc). The presence of an  $\alpha$ 1-4-linked fucose in A-

heptasaccharide (GalNAc $\alpha$ (L-Fuca2)3Gal $\beta$ (L-Fuc $\alpha$ 4) 3GlcNAc $\beta$ 3Gal $\beta$ 4Glc) reduces the affinity. Binding reactions are enthalpically driven. Failure to observe appreciable conformational rearrangement(s) for either protein or sugar as well as the complexity and the linearity of Van't Hoff plots for each of the sugars examined indicate that these interactions are accompanied by little heat capacity changes. This, together with enthalpy-entropy compensation observed for these processes, underscores the importance of water reorganization being one of the principal determinants of protein-sugar interactions and the important part played by sugars, not involved directly in binding, in favourably orienting the interacting regions of sugars<sup>2</sup>.

### 2.2. Extrinsic fluorescence thermodynamic analysis of the binding of 4-methylumbelliferyl glycosides

The interaction between the 4-methylumbelliferyl glycosides of galactose and N-acetylgalactosamine was performed to probe the role of bulkier substituents at the anomeric position and at C-2 carbon of galactose. It was observed that upon binding to WBA I, MeUmb- $\alpha$ -galactosides show quenching in fluorescence intensity, decrease in UV absorbance with a concomitant blue shift and decrease in fluorescence excited-state lifetimes. However, their  $\beta$ -analogues show enhancement in fluorescence intensity, increase in UV absorbance with a red shift and an increase in fluorescence excited-state lifetimes, implying that the anomeric configuration of the galactoside residues bound to WBA I leads to a major change in the binding of the fluorophore. The 4-methylumbelliferyl group contributes positively to the affinity of these saccharides for WBA I and tends to mask the anomeric discriminatory power of WBA I as compared to methyl or a glycon group such as glucose. The binding of MeUmb- $\beta$ -galactosides to WBA I is accompanied with a large enthalpic contribution, whereas MeUmb- $\alpha$ -galactosides show an entropically favourable binding. Substitution of the hydroxyl group at C-2 carbon of galactose by an acetamido group leads to the stabilization of the lectin-MeUmb-galactoside complex, mainly due to a large favourable entropy change, suggesting that the acetamido group at C-2 of galactose binds to a relatively non-polar subsite of the lectin<sup>4</sup>.

### 2.3. Stopped-flow spectrofluorimetric studies

The effect of the bulkier substituent, at the anomeric position and at C-2 carbon of galactose, on the elementary steps involved in the interaction of 4-methylumbelliferyl glycosides of galactose and N-acetylgalactosamine to WBA I was monitored by the sugar specific change in the fluorescence of the umbelliferyl fluorophore by stopped-flow spectrofluorimetry. The kinetics follow an one-step binding mechanism and the second-order rate constants are slower than the diffusion-controlled process. An interesting feature noted for the first time in protein-sugar interactions is the dependence of the second-order rate constants for the binding of WBA I to MeUmb-galactosides on the nature of the substituent at C-2 carbon of galactose as well as on the nature of the linkage of the aglycon 4-methylumbelliferyl moiety. Substitution of the hydroxyl group at C-2 of galactose by a bulky acetamido group reduces the association rate constant dramatically. An inspection of the activation parameters reveals that the enthalpy of activation is the limiting factor for the differences in the forward rate constants for these saccharides and the entropic contribution to the activation energy is small. Relatively slower binding of GalNAc $\beta$ MeUmb and GalNAc $\alpha$ MeUmb is presumably due to a requirement of considerable reorientation of water molecules around acetamido group and/or the corresponding *loci* from the protein<sup>5</sup>.

### 2.4. Titration calorimetric studies

Titration calorimetric studies were undertaken to elucidate directly the thermodynamics of the WBA I-galactoside interaction in more detail. These results show that both the binding sites of WBA I are independent and equivalent. The binding reactions are essentially enthalpically driven and for the most part occur with little change in the heat capacity ( $dH_b/dT = 0$ ), implying that the binding mechanism involves a simple bimolecular reaction driven by the van der Waals interactions between the sugar and the protein at the binding site with little or no structural change in WBA I<sup>6</sup>.

### 2.5. Differential scanning calorimetry (DSC)

DSC was used to study the domain structure of WBA I and their interaction in the protein and with the ligands. Conformation of WBA I and the conformational changes induced by different galactosides was monitored by the transition temperature ( $T_m$ ) in the presence of different ligands. Denaturation transition of WBA I consisted of two

overlapping peaks over the pH range 5.6–7.4. Fits of the DSC data to a two-state transition model showed that the low-temperature transition ( $341.6 \pm 0.4$  K at pH 7.4) consisted of two domains unfolding as a single entity while the higher temperature transition ( $347.8 \pm 0.6$  K at pH 7.4) is of the remaining WBA I dimer unfolding into two monomers. Both transitions shift to higher temperatures and higher calorimetric enthalpies with increase in added ligand concentration at pH 7.4. Analysis of the temperature increase as a function of added ligand concentration suggests that one ligand binds to the two domains unfolding at  $341.6 \pm 0.6$  K and one ligand binds to the domain unfolding at  $347.8 \pm 0.6$  K. Upon binding of sugar ligands to WBA I, the thermal stability of all three thermodynamic domains increases and the multi-domain structure remains the same. The presence of multi-thermodynamic domains in WBA I would imply that the secondary and/or tertiary structural elements in WBA I exhibit less interactions between the amino acid residues<sup>6</sup>.

### 2.6. Complete amino acid sequence determination

The primary structure of WBA I was determined to derive information about the origin of its non-symmetrical domain organization. The complete amino acid sequence was obtained by a combination of manual and gas phase sequencing methods. Peptide fragments for sequence analyses were obtained by enzymatic cleavages using trypsin, *Staphylococcus aureus* V<sub>8</sub> protease and chemical cleavages by iodosobenzoic acid, hydroxylamine and formic acid. C-terminal sequence analysis of WBA I and other peptides was performed using carboxypeptidase Y. The primary structure of WBA I was homologous to other legume lectins, more so to *Erythrina corallodendron*. Interestingly, the lectin sequence is almost identical to the *Erythrina corallodendron* lectin's regions involved in the association of its two monomers. Other conserved regions are the double metal-binding site, residues contributing to the formation of the hydrophobic cavity and carbohydrate binding site. The consensus sequence, LQRD, for targeting of proteins to vacuoles is also observed in WBA I and it has only one glycosylation site (N218) which is quite close to the carboxy-terminus<sup>7</sup>.

### 3. Conclusion

The primary structure of WBA I shows that it belongs to the family of single-chain legume lectins. The overall features of legume lectins are conserved in WBA I. The amino acid differences in the carbohydrate binding loop are related to its sugar specificity. The differences with other legume lectins are also concerned with glycosylation site and proline-rich sequence motif. In addition, the data also provide a preliminary framework for the understanding of the unusual thermodynamic behaviour of WBA I and about the protomer–protomer interface in other legume lectins.

### References

1. LIS, H. AND SHARON, N. *A. Rev. Biochem.*, 1986, 55, 36–67.
2. MATSUDA, T., KABAT, E. A. AND SUROLIA, A. *Mol. Immunol.*, 1989, 26, 189–195.
3. KHAN, M. I., SASTRY, M. V. K. AND SUROLIA, A. *J. Biol. Chem.*, 1986, 261, 3013–3019.
4. PURI, K. D., GOPALAKRISHNAN, B. AND SUROLIA, A. *FEBS Lett.*, 1992, 312, 208–212.
5. PURI, K. D., KHAN, M. I., GUPTA, D. AND SUROLIA, A. *J. Biol. Chem.*, 1993, 268, 16378–16387.
6. SCHWARZ, F. P., PURI, K. D. AND SUROLIA, A. *J. Biol. Chem.*, 1991, 266, 24344–24350.
7. PURI, K. D. AND SUROLIA, A. *J. Biol. Chem.*, 1994, 269, 30917–30926.

Thesis Abstract (Ph. D.)

Molecular modelling studies on wheat germ agglutinin–saccharide interactions by S. Mohan

Research supervisor: V. S. R. Rao  
Department: Molecular Biophysics Unit

### 1. Introduction

Wheat germ agglutinin (WGA), a plant lectin from wheat (*Triticum vulgare*), binds specifically to N-acetyl glucosamine (GlcNAc) and N-acetyl neuraminic acid (NeuNAc) containing saccharides<sup>1-2</sup>. Since these sugars commonly occur on the cell surface, WGA has been used as a probe to study various properties of cells associated with the complex carbohydrates which are present on their outer surface. The properties which have been studied include malignancy, cell growth, differentiation, etc.

Under physiological condition WGA exists as a dimer. Equilibrium-dialysis measurements have suggested that the WGA monomeric unit contains two identical and independent binding sites for GlcNAc and its  $\beta(1 \rightarrow 4)$ -linked oligomers. X-ray diffraction studies have revealed that these sugar-binding sites are located at the interface between two monomers (four/dimer) and are termed as primary and secondary sites based on their accessibility to solvent molecules. Among the simple saccharides tested for inhibition, GlcNAc binds better than the other monosaccharides, NeuNAc and GalNAc. These studies also have indicated increased affinity for  $\beta(1 \rightarrow 4)$ -linked di-N-acetyl glucosamine (GlcNAc)<sub>2</sub> and tri-N-acetyl glucosamine (GlcNAc)<sub>3</sub> compared to that for the GlcNAc residue alone<sup>3</sup>. The affinity of these oligosaccharides for the lectin increases with size; the disaccharide being over one hundred and the trisaccharide one thousand times more tightly bound than GlcNAc. These findings have been confirmed by fluorescence quenching and UV difference absorption spectrometry.

Complexes of WGA with the  $\beta(1 \rightarrow 4)$ -linked disaccharide of N-acetyl glucosamine have been analysed using X-ray diffraction technique<sup>4</sup>. These crystals are, however, unstable and mild glutaraldehyde treatment was used to stabilise them. Analysis of the X-ray data of the glutaraldehyde cross-linked WGA crystals soaked with (GlcNAc)<sub>2</sub> reveals the presence of two unique binding sites (four/dimer). In contrast to the difficulties with (GlcNAc)<sub>2</sub> complexes, WGA crystals are stable in the presence of neuraminylactose. In solid state, two molecules of neuraminylactose bind at the primary sites of the WGA<sup>5</sup>. Binding of this saccharide at the secondary sites of WGA has not been observed in solid state. However, a high-resolution NMR study indicates that in solution WGA binds four molecules of N-acetyl neuraminylactose.

Recently, molecular modelling techniques have been extended to generate the possible three-dimensional structures of unknown complexes using the known structure of the native protein. In the present work, an attempt has been made to generate the possible three-dimensional structure of various complexes of WGA using molecular modelling and energy optimisation techniques.

### 2. Method of calculation

A three-step molecular modelling has been used to study the conformation of saccharides and their interaction with WGA. The steps are:

- (i) Exploration of conformational space and energies of saccharide inhibitors of WGA using molecular dynamics technique.
- (ii) Determination of stereochemically allowed orientations of the ligand in the binding site of the protein by contact criteria.
- (iii) Minimisation of the potential energy of the protein-saccharide complexes in torsion angle and rigid body parameter space.

### 3. Results and discussion

Molecular dynamics studies on monosaccharide inhibitors have shown that at room temperature, both in vacuum and in the presence of water, the sugar ring can exhibit limited flexibility with fluctuations centred around the <sup>4</sup>C<sub>1</sub> conformation for GlcNAc and GalNAc and <sup>2</sup>C<sub>5</sub> conformation for NeuNAc. However, at high temperature the sugar ring readily undergoes transition from one chair conformation to another via different boat conformations. This study demonstrates the high flexibility of the side group hydroxyls and indicates a preference for them to

form hydrogen bonds with water molecules rather than forming intra molecular hydrogen bonds. It also reveals the possibility of glycerol side group of NeuNAc existing in an extended as well as bent conformer with the former being the predominant one.

MD studies on oligomers of GlcNAc indicate that these molecules are flexible and the inter-unit dihedral angles ( $\phi$ ,  $\psi$ ) generally fluctuate rapidly in a limited region. Hence, these molecules may not exist in any discrete conformation in solution. The solvent water affects significantly the orientation of the hydroxymethyl group and possible inter and intra hydrogen bonds. It also dampens the fluctuations in ( $\phi$ ,  $\psi$ ) and restricts them to a very narrow region.

MD studies on monosialogangliosides have shown that the inclusion of water molecules in the simulation restricts the frequency of transition from one conformer to another. This study clearly shows that in GM3 and GM4 the NeuNAc-Gal fragment favours conformations around ( $-80^\circ$ ,  $-10^\circ$ ) and ( $-150^\circ$ ,  $-20^\circ$ ) while the latter is favoured only in the case of GM2 and GM1. This is in agreement with NMR studies.

The calculated binding energies of GlcNAc, GalNAc and ManNAc with WGA explain the experimental studies that GlcNAc binds better than GalNAc and ManNAc. The GalNAc may bind to WGA in nearly the same orientation as that of GlcNAc at both the primary and secondary sites, whereas ManNAc binds in totally different orientation. This study has shown that NeuNAc binds equally well at the primary site and weakly at the secondary site compared to GlcNAc. Interestingly, in the preferred conformer NeuNAc and GlcNAc have similar hydrogen-binding schemes only at the primary sites.

In the (GlcNAc)<sub>3</sub>-WGA complex having the saccharide at either primary or the secondary site, the hydrogen bond scheme predicted for the lowest energy conformer agrees with the models proposed by C. S. Wright for the non-reducing sugar with the protein. However, in addition to the hydrogen bonds proposed by C. S. Wright the present study also suggests the possibility of additional hydrogen bond interactions between middle and reducing sugars. These interactions perhaps explain the higher affinity of (GlcNAc)<sub>3</sub> and (GlcNAc)<sub>2</sub> over GlcNAc. In all the monosialogangliosides-WGA complexes, NeuNAc fragment favourably interacts with WGA both at the primary and secondary sites suggesting the importance of NeuNAc at the interior of the binding site.

## References

1. PRIVAT, J. P., DELMOTTE, F. AND MONSIGNY, M. *FEBS Lett.*, 1974, 46, 229-232.
2. LIS, H. AND SHARON, N. *A. Rev. Biochem.*, 1986, 55, 229.
3. NAGATA, Y. AND BURGER, M. M. *J. Biol. Chem.*, 1974, 249, 3116.
4. WRIGHT, C. S. *J. Mol. Biol.*, 1987, 194, 501.
5. WRIGHT, C. S. *J. Mol. Biol.*, 1990, 215, 635.

## Thesis Abstract (Ph. D.)

**Studies on the synthesis, structure and reactivity of amino and halo silanes by K. N. Radhamani**

Research supervisor: D. K. Padma

Department: Inorganic and Physical Chemistry

### 1. Introduction

The chemistry of organo and halo silanes is an important field which provides an active area of both fundamental and technological research. In organo silicon chemistry, the silicon-nitrogen compounds embrace both inorganic and organic chemistry<sup>1</sup>. The current status of knowledge indicates that except for a few tri(amino)

silanes, there is little information available concerning their studies<sup>2</sup>. It was therefore considered worthwhile to explore the different methods for their syntheses, reactivity and the various factors that govern their spectroscopic properties.

## 2. Present study

The objective of the present study is to understand the nature of silicon nitrogen and halogen bonds. As a result, the synthesis and spectral studies of various tri(amino)silanes,  $(R_2N)_3SiH$ , have been carried out. The condensation reaction of trichlorosilane with secondary amines- $(R_2NH)$ ; (1) pyrrolidine, (2) piperidine, (3) hexamethylenimine, (4) morpholine, (5) N-methylpiperazine, and (6) diethylamine gave  $(R_2N)_3SiH$ , while the transamination reactions of tris(diethylamino)silane with the above-mentioned amines resulted in the formation of mixed amino derivatives  $(Et_2N)_2(R_2N)SiH$ ,  $(Et_2N)(R_2N)_2SiH$  as well as  $(R_2N)_3SiH$ . The synthesized compounds were characterized by IR, ( $^{29}Si$ ,  $^1H$ ) NMR, and CHN analysis.

On analysing the results it was noted that the  $^{29}Si$  NMR chemical shifts of these compounds show appreciable change in their chemical shifts though the pKa values of the unsubstituted amines are similar. The deviation can be accounted for by the change in the orientation of the nitrogen lone pair which affects the donation of it to the vacant 'd' orbitals of silicon. It has also been observed that the IR stretching frequency of the Si-H bond varies in a narrow range of  $2104 \pm 3 \text{ cm}^{-1}$ . The theoretical frequency of the Si-H bond has been calculated by using an empirical equation,  $\nu_{Si-H} = 1512.77 + 39.7\Sigma SR$ , where  $\Sigma SR$  is the group electronegativity sum and are calculated from Pauling's electronegativity scale. A plot of the calculated and observed  $\nu_{Si-H}$  vs group electronegativity shows that the above equation holds good for these derivatives.

An attempt was made to prepare the mixed amino silanes using a mixture of amines and this reaction always resulted in the formation of a single product, having the least steric hindrance. However, a new synthesis presently developed was effective in isolating the mixed amino derivatives in good yields and high purity. Transamination reactions show it to be a good route for the synthesis of mixed amino derivatives. Sterically hindered mixed tri(amino)silanes have been prepared by the transamination of tris(dicyclohexylamino)silane,  $HSi(DCA)_3$ , (obtained by the condensation of trichlorosilane and dicyclohexylamine) and other secondary amines to form the following types of products:  $(DCA)(R_2N)_2SiH$  and  $(DCA)_2(R_2N)SiH$ . The IR-stretching frequency of  $(DCA)(R_2N)_2SiH$  series appears in the range  $2116-2134 \text{ cm}^{-1}$ . A correlation of the Si-H frequencies vs the group electronegativity shows that for  $(DCA)_2(R_2N)SiH$  the observed and calculated values differ to a large extent. The  $^{29}Si$  chemical shifts of mixed amino derivatives show appreciable change even though the unsubstituted amines have similar pKa. This perhaps may be due to the fact that as steric bulkiness of the substituent increases, the electron donation may not be very efficient as in the case of small systems.

Two selected derivatives have been taken for (single-crystal X-ray analysis) studying the structural features of bonding of the amino silanes. The single crystal structure of tris(morpholino)silane reveals that there is no appreciable difference in various Si-N bond lengths. One of the nitrogens is slightly pyramidal (total angle around nitrogen =  $356.7^\circ$ ), while the other two are essentially planar. Structural study on another sterically hindered derivative  $((C_6H_{11})_2N)(C_6H_{12})_2SiH$  reveals that one of the Si-N bond lengths is slightly shorter than the other two. Also the nitrogens are slightly more pyramidal than the morpholino derivative. The  $^{15}N$  NMR spectrum of these two compounds reveals that two of the nitrogen atoms are in the same environment while the third one is slightly different, as also evident from the crystallographic studies.

The Newman projection diagram of these compounds shows that one of the nitrogen lone pairs is oriented at an angle of  $180^\circ$  with Si-H. Hence this lone pair can have effective conjugation with Si-H bond, whereas the two lone pairs of the other two nitrogens are oriented at  $180^\circ$  with Si-N bonds and hence will have mutual interactions. This is evident from the  $^{15}N$  NMR spectrum, where two of the nitrogens have the same chemical shift and the third one is different. The same situation prevails in the other compound also. But the orientation of the nitrogen lone pair which is anti to Si-H bond is slightly reduced from  $180^\circ$ . The nitrogens are slightly more pyramidal in this compound. As a result, the interaction of the nitrogen lone pair with the silicon 'd' orbital is decreased. This study provides the evidence that in more bulky systems there is the possibility of the nitrogen being more pyramidal, thereby showing an increasing hyperconjugative interaction of the nitrogen lone pair with Si-N bond.

The results obtained in the above crystallographic data were further proved by theoretical calculations (MNDO), using model system  $\text{HSi}(\text{NH}_2)_3$ . Substitution of the N-H, hydrogen with methyl groups reveals that the charge on the silicon and nitrogens remains the same as that of  $\text{HSi}(\text{NH}_2)_3$ . This implies that it is not the electron-donating power of the substituent that decides the charge on the various atoms but the geometry around the nitrogen also plays a key role in determining the charges. In the totally planar form the lone pairs are exactly perpendicular to Si-H bond thereby showing the absence of hyperconjugation with these bonds. But in the completely pyramidal form the orientation of the lone pair is such that each of the nitrogen lone pairs can overlap with any one of the other two Si-N bonds resulting in hyperconjugation. The Si-N bond lengths are 1.77 Å in pyramidal form and 1.71 Å in the planar form. This change in bond length is probably due to the hyperconjugative interaction in the former and (p-d)  $\pi$  interaction in the latter. From the above results, it is very clear that structure and bonding in tri(amino)silanes depend on the size of the amine which in turn determines the orientation of the nitrogen lone pair.

Fluorination of tri(amino), alkyl and chloro silanes using pyridinium poly(hydrogen fluoride) shows an interesting variety of cleavage reactions indicated by the fission of Si-N, Si-H, Si-C and Si-Cl bonds<sup>4</sup>. The tetravalent silicon becomes hexavalent thereby showing the expansion of the coordination number of silicon with incorporation of fluoride ions resulting in a variety of cations being associated with hexafluorosilicates  $((\text{R}_2\text{NH})_2\text{SiF}_6)^+$ .

The thermal decomposition of tri(amino)silanes in an inert atmosphere/ $\text{NH}_3$  has been carried out and the analysis of the product shows the presence of  $\beta\text{Si}_3\text{N}_4$ . The hydrolysis and alcoholysis of tri(amino)silanes gave rise to silica and tetramethoxysilane. A few reactions have been carried out to check the reducing activity of the Si-H hydrogen, in the presence of a catalyst, KF. The results indicate that tri(amino)silanes are efficient reducing agents and reduce carbonyl and P=O groups. The reactivity of tri(amino)silanes with phosphines has been carried out. The products showed a mixture of phosphines and tri(amino)silanes, which indicates that the Si-N bond can be substituted.

Thus, trichlorosilanes form pure and mixed tri(amino)silanes. These tri(amino)silanes exhibit special bonding features. They have been found to be good reducing agents and are highly reactive towards phosphines and alcohols. In addition, these compounds could be used as good starting materials for the preparation of non-oxide ceramics ( $\beta\text{Si}_3\text{N}_4$ ).

## References

1. FESSENDEN, R. and FESSENDEN, J. S. The chemistry of silicon-nitrogen compounds, *Chem. Rev.*, 1961, 61, 361.
2. EGOROCHKIN, A. N. AND KHORSHEV, S. YA. Spectroscopic study of steric effects in organic compounds of silicon subgroup elements, *Russ. Chem. Rev.*, 1980, 49, 820.
3. REED, A. E. AND SCHLEYER, P. V. R. The anomeric effect with central atoms other than carbon. 2. Strong interactions between non-bonded substituents in mono- and poly-fluorinated first and second row amines  $\text{F}_n\text{AH}_m\text{NH}_2$ , *Inorg. Chem.*, 1988, 27, 3969.
4. KALBANDKERI, R. G., SYED MOHAMMED, K., PADMA, D. K. AND VASEUDEVA MURTHY, A. R. A new synthetic procedure for the preparation of pyridinium tetra-fluoroborate and hexafluorosilicate, *Polyhedron*, 1985, 4, 787.

Thesis Abstract (Ph. D.)

**Infrared and Raman spectroscopic investigations of phase transitions in complex solids by Vijay Varma**

Research supervisor: C. N. R. Rao

Department: Solid State and Structural Chemistry Unit

### 1. Introduction

Infrared and Raman spectroscopic techniques probe vibrational excitations in a solid and provide useful information on structure and dynamics. These techniques have been very useful towards the understanding of the microscopic mechanism of phase transitions in solids<sup>1</sup>. This thesis deals with investigations of phase transitions in a variety of complex solids.

### 2. Experimental

Infrared spectroscopic investigations were carried out with either powdered samples dispersed in KBr and polyethylene matrices or with neat samples between CsI, KBr or KRS-5 windows, employing a Bruker IFS 113V FTIR spectrometer. Raman spectra were recorded with a Spex 1403 laser Raman spectrometer employing a Spectra Physics argon ion laser for excitation. Variable-temperature studies were carried out using an Air Products cryogenic refrigeration system and a Specac variable-temperature assembly.

### 3. Results and discussion

Investigations of methylammonium haloantimonates(III), represented by the general formula  $[\text{N}(\text{CH}_3)_{4-n}\text{H}_n]_3\text{Sb}_2\text{X}_9$  ( $n = 0-3$ ,  $\text{X} = \text{Cl}$  or  $\text{Br}$ ), and halobismuthates(III),  $(\text{CH}_3\text{NH}_2)_3\text{Bi}_2\text{Br}_9$  and  $(\text{CH}_3\text{NH}_2)_3\text{Bi}_2\text{Br}_{11}$ , show that there is dynamic disorder of methylammonium cations in the high-temperature phases. On cooling, phase transitions are caused by freezing out of the rotational motions of methylammonium cations. The cation orientations are stabilized by hydrogen bonds. At still lower temperatures motions of cation and anion couple through hydrogen bonds and drive different types of phase transitions<sup>2</sup>.

A study of phase transitions in hydrozonium sulfate,  $\text{N}_2\text{H}_6\text{SO}_4$ , shows that in the room-temperature phase, hydrogen bonding causes distortions of hydrozonium ( $\text{N}_2\text{H}_6^{2+}$ ) and  $\text{SO}_4^{2-}$  ions. The high-temperature phase (above 483 K) is without hydrogen bonding,  $\text{N}_2\text{H}_6^{2+}$  and  $\text{SO}_4^{2-}$  ions being undistorted. In this phase hydrozonium ion is also rotationally disordered. The low-temperature phase (below 230 K) results from a rearrangement of hydrogen bonds. Torsional barrier for the hindered integral rotation in  $\text{N}_2\text{H}_6^{2+}$  was calculated to be around  $32 \text{ kJ mol}^{-1}$  which is very high compared to that in ethane. This is attributed to the effects of hydrogen bonding and solid state<sup>3</sup>.

Cesium hydrogen sulfate,  $\text{CsHSO}_4$ , becomes superionic conductor above 417 K. Infrared and Raman spectra reflect the high disorder of this phase. Effect of lithium substitution is similar to that of heating  $\text{CsHSO}_4$ . With 30% lithium substitution the degree of disorder is intermediate between the room temperature and the superionic phase. The  $\text{HSO}_4^-$  libration mode shows softening with respect to temperature as well as lithium substitution<sup>4</sup>.

An infrared spectroscopic investigation of solid  $\text{C}_{70}$  shows that this solid undergoes two phase transitions around 340 and 280 K. These transitions are associated with orientational ordering of  $\text{C}_{70}$  molecules. Freezing of rotational motions of  $\text{C}_{70}$  molecules about the long and short axes occurs at different temperatures. Energetically close phases coexist in the low-temperature region<sup>5</sup>.

Cyclic phosphazene tetramer,  $\text{P}_4\text{N}_4\text{Cl}_8$ , exhibits conformational polymorphism. Normal mode assignments support that the high-temperature form has skew-chair ( $\text{C}_{2h}$ ) and the low-temperature form has skew-tub ( $\text{S}_4$ ) conformations of the molecule. The phase transition of  $\text{P}_4\text{N}_4\text{F}_8$  around 200 K has been found to be associated with softening of a low-frequency mode<sup>6</sup>.

An infrared spectroscopic study of  $\text{Fe}_{1-x}\text{Mn}_x(\text{Phen})_2(\text{NCS})_2$  shows that the first-order nature of the spin cross-over phase transition in  $\text{Fe}(\text{Phen})_2(\text{NCS})_2$  is diluted on  $\text{Mn}^{2+}$  substitution and the transition becomes second order with increasing  $\text{Mn}^{2+}$  substitution. High-spin state is stabilised even at very low temperatures with increasing  $\text{Mn}^{2+}$  substitution<sup>7</sup>.

### References

1. IQBAL, Z. AND OWENS, F. J. (Eds) *Vibrational spectroscopy of phase transitions*, 1984, Academic Press.

2. VARMA, V., BHATTACHARJEE, R., VASAN, H. N. AND RAO, C. N. R. *Spectrochim. Acta A*, 1992, 48, 1631.
3. VARMA, V. AND RAO, C. N. R. *J. Mol. Struct.*, 1992, 268, 1.
4. VARMA, V., RANGAVITTAL, N. AND RAO, C. N. R. *J. Solid St. Chem.* (to be published).
5. VARMA, V., SESHADRI, R., GOVINDRAJ, SOOD, A. K. AND RAO, C. N. R. *Chem. Phys. Lett.* (to be published).
6. VARMA, V., FERNANDES, J. R. AND RAO, C. N. R. *J. Mol. Struct.*, 1989, 198, 403.
7. VARMA, V. AND FERNANDES, J. R. *Chem. Phys. Lett.*, 1990, 167, 367.

### Thesis Abstract (Ph. D.)

## Algorithms to test and implement fault tolerance in self-routing permutation networks by S. Ravi Shankar

Research supervisor: Lawrence Jenkins

Department: Electrical Engineering

### 1. Introduction

Self-routing permutation networks (SRPNs) constitute a subclass of multistage interconnection networks, and have been used in several multiprocessor systems to provide interprocessor, processor-to-memory and processor-to-I/O communication<sup>1</sup>. As the occurrence of even a single fault renders an SRPN useless, much effort has gone into testing and implementing fault tolerance in it. These methodologies are however restrictive because they apply either to specific instances of or to subclasses such as the class of baseline equivalent networks<sup>2</sup>. These restrictions arose due to the nonavailability of a suitable SRPN model. Recently, a matrix model was proposed for SRPNs<sup>3</sup>. However, this model is not conducive for deriving general methodologies for testing and implementing fault tolerance because of its complexity.

### 2. Contribution of the thesis

This thesis proposes a model for SRPNs based on the concept of hierarchical routing. Several interesting topological properties of SRPNs have been identified and used to develop techniques to implement fault tolerance in SRPNs.

The best known testing technique for SRPNs is due to Feng and Wu. However, this technique is valid only for baseline equivalent networks<sup>4</sup>. This technique assumes a realistic fault model, and has been used to develop a general scheme for testing.

A test algorithm called color-link, based on the concept of edge coloring in graphs, has been developed. It has been proved that the Feng and Wu algorithm is a special case of this general algorithm.

A test called design for testability (DFT) has been developed to determine whether the switching elements (SEs) in an SRPN could be set in constant time for testing. A technique called Redesign has been presented to modify SRPNs so that they pass the DFT.

The detection and location of single faults has also been addressed. In fault location, the stage containing the fault is identified using one of two algorithms—Triangulation and Binary-Search; the faulty component is then identified through backtracking.

Fault tolerance in SRPNs can be implemented through logical or physical techniques. One of the logical techniques is dynamic full accessibility (DFA)<sup>5</sup>. In DFA, if the direct path between two processors becomes faulty, communication is established through other processors connected to the SRPN. It has been shown that an earlier method<sup>5</sup> to check for DFA is incorrect.

In this thesis, a faulty SRPN has been modelled as a digraph, and it has been shown that testing a faulty SRPN for DFA is equivalent to testing the corresponding digraph for strong connectedness. Two algorithms have been proposed for this. One of these, called Log-Step, is based on Harary's theorem from graph theory and the other, Fuse, is based on the concept of vertex compression. Both these algorithms make use of the reachability matrix of the digraph of the faulty SRPN. An optimal test called R-Construct has therefore been developed to obtain the reachability matrix from the faulty SRPN. The algorithm Fuse has been shown to support graceful degradation.

An algorithm for routing under DFA has also been proposed. This algorithm called Table-Update makes use of the reachability matrix and is based on the concept of depth-first search.

Physical techniques achieve fault tolerance through redundant hardware. Two such techniques called extrastaging<sup>6</sup> and chaining<sup>7</sup> have been discussed in this thesis. In extrastaging, an extra switching stage is added to an SRPN to provide redundant paths between every pair of input and output terminals. Fault tolerance in chaining is achieved through intrastage interconnections.

It has been shown that extrastaging cannot be applied to all SRPNs. A necessary and sufficient condition for an SRPN to be extrastageable has been developed. A test to check for this condition has also been proposed. For SRPNs which pass this test, techniques have been developed to design the corresponding extrastaged network such that the addition of the extra switching stage does not affect the desired function of the SRPN. Testing extrastaged SRPNs and routing in them has also been addressed.

This thesis shows that chaining involves interconnecting the nodes at every level in every reverse tree<sup>8</sup> of an SRPN. The issue of designing a chaining scheme in which the routing delay is minimal and robustness is maximized has also been addressed. To achieve this, the partitions of an SRPN have to be identified. An algorithm has been developed for this. Another algorithm called CALM (Chaining ALgorithm) has been developed to design chained networks with minimal routing delay and maximal robustness.

The algorithms for fault tolerance discussed in this thesis are applicable to all SRPNs, regardless of their size or topology.

## References

1. HWANG, K. AND BRIGGS, F. A. *Computer architecture and parallel processing*, 1985, McGraw-Hill.
2. WU, C. AND FENG, T. Y. On a class of multistage interconnection networks, *IEEE Trans.*, 1980, C-29, 694-702.
3. NAVANEETHAN, P. *BIPEDS: A new class of self-routing permutation networks for array processing systems*, Ph. D. thesis, Deptt of Elect. Engng, Indian Institute of Science, Bangalore, India, 1991.
4. FENG, T.-Y. AND WU, C. Fault diagnosis in a class of multi-stage interconnection networks, *IEEE Trans.*, 1981, C-30, 743-757.
5. AGARWAL, D. P. AND LEU, J. S. Dynamic accessibility testing and path length optimization, *IEEE Trans.*, 1985, C-34, 255-266.
6. ADAMS III, G. B. AND SIEGEL, H. J. The extra stage cube: A fault tolerant interconnection network for supersystems, *IEEE Trans.*, 1982, C-31, 443-454.
7. TZENG, N-F. *et al.* Realizing fault tolerant interconnection networks via chaining, *IEEE Trans.*, 1988, C-37, 458-462.
8. AGARWAL, D. P. Graph theoretical analysis and design of multistage interconnection networks, *IEEE Trans.*, 1983, C-32, 637-648.

## Thesis Abstract (Ph. D.)

**Analysis of some smoothing techniques with application to narrowband/broadband beamforming and DOA estimation by K. C. Indukumar**

Research supervisor: V. U. Reddy

Department: Electrical Communication Engineering

**1. Introduction**

The performance of direction-of-arrival (DOA) estimation and beamforming algorithms degrades in the presence of correlated signals in both narrow- and broadband cases. We encounter the correlated signals in situations like multipath propagation and smart jamming environment where several or all of the impinging signals are either partially or fully correlated. Several methods have been proposed for decorrelating narrowband signals prior to DOA estimation and beamforming. Preprocessing techniques like spatial smoothing and weighted smoothing which preserve the underlying structure of the signal model were proposed to decorrelate narrowband signals. The effect of progressive smoothing and its impact on DOA estimation and beamforming was studied by Reddy *et al.*<sup>1</sup>. Recently, Linebarger *et al.*<sup>2</sup> proposed redundancy averaging as an alternative preprocessing method which uses full aperture of the array, in contrast to other smoothing methods.

The performance of the DOA estimation algorithms degrades when we work with finite data, and degrades further if the signals are correlated. Smoothing techniques have been proposed to improve the performance. In spatial smoothing, all the subarray covariances are equally weighted and a simple averaging is performed. Recently, the finite data performance of the MUSIC and minimum norm methods with spatial smoothing has been analyzed and an expression for the mean-squared-error (MSE) in the DOA estimates has been derived<sup>3,4</sup>.

In the context of narrowband signals, analysis and comparison of different algorithms have been done with respect to measures like the extent of correlation and the rate of decorrelation. The correlation measure used in the narrowband case does not apply to the broadband signals. Hence, there is a need to develop a measure which reflects the correlation between the signals in the broadband case.

**2. Results**

Recently, redundancy averaging has been proposed as an alternative preprocessing method which does not suffer from reduced aperture. Considering asymptotic data case, it is shown analytically that this technique results in an eigenstructure which is inconsistent with that of the underlying signal model. A two-source case is first analyzed for simplicity and later extended to D-source case. It is shown, in particular, that the resulting subspace fills up the whole M-dimensional space, where M is the array size, and the resulting covariance matrix is not guaranteed to be non-negative definite. As a result of spreading of the signal subspace, subspace-based methods like MUSIC induce bias in the DOA estimates.

Correlation between the signals and the finite data causes degradation in the performance of beamforming and DOA estimation algorithms. Smoothing techniques are normally used to improve the performance in these situations. Smoothing, in general, refers to weighted averaging of all the subarray covariance matrices prior to the application of DOA estimation algorithms. A generalized subarray covariance weighting scheme is formulated and a minimization procedure is developed for computing the set of optimum weights which gives minimum MSE in the DOA estimates for the case of MUSIC and minimum-norm methods in finite data. Using this optimum weighting, a trade-off between the subarray size and the number of subarrays is studied. Since the computation of optimum weights requires exact scenario parameters (which are not available in practice), two methods are suggested to estimate these weights with the available finite data. In the first method, the scenario parameters are estimated from the observed data and they are used in place of the true ones. The second method is based on the observation that the optimum weights have a pattern which resembles Taylor weights pattern. A method is proposed to choose an appropriate set of Taylor weights which serve as near-optimum weights for moderately wide range of scenarios.

The usage of magnitude of coefficient of correlation is a well-known measure of correlation in the narrowband case. However, there is no such measure in the broadband case. A new measure of correlation between broadband signals is proposed. This measure is the Frobenius norm of the cross-correlation part of the data covariance matrix. It is shown that the new measure is indeed a measure of correlation. Using this measure, the effect of multipath delay on the correlation is studied. To study the decorrelating effect of smoothing as a function of various parameters, an upper bound on the F-form measure is developed. The effect of spacing and direction of the sources on the rate of decorrelation with progressive smoothing is studied for the broadband case using this bound.

Spatial smoothing technique decorrelates the signals only asymptotically with the number of subarrays. To achieve perfect decorrelation with finite number of subarrays, a weighted smoothing method based on Toeplitz-block-Toeplitz (TBT) structuring of the data covariance matrix is proposed which yields near-perfect decorrelation for a finite number of subarrays. The weights are chosen so as to minimize the sum of squared deviations of the elements in the weighted subarray covariance matrix from those of TBT matrix. The rate of decorrelation in TBT structuring method is shown to be much faster compared to that obtained with spatial smoothing.

#### References

1. REDDY, V. U., PAULRAJ, A. AND KAILATH, T. *IEEE Trans. ASSP*, 1987, 35, 927-936.
2. LINEBARGER, D. A. AND JOHNSON, D. H. *IEEE Trans. ASSP*, 1990, 38, 880-884.
3. PILLAI, S. U. AND KWON, B. H. *IEEE Trans. ASSP*, 1989, 37, 1176-1189.
4. RAO, B. D. AND HARI, K. V. S. *Proc. IEE, Part F*, 1990, 137, 449-458.

#### Thesis Abstract (Ph. D.)

### Design and performance study of a media access control protocol for wireless LANs

by A. Chockalingam

Research supervisors: P. Venkataram and A. Prabhakar (ITI)

Department: Electrical Communication Engineering

#### 1. Introduction

Computer communication networks have so far been implemented and used mainly over physical cabling that interconnects desktop personal computers and workstations. Recently, wireless data communications using radio transmission medium and portable computers are increasingly becoming part of networks<sup>1,2</sup>. Wireless solutions are also adopted for library and factory automation networks to overcome the problem of laying interconnecting local area network (LAN) cables within and across buildings<sup>3,4</sup>.

Optimal sharing of a common transmission medium by multiple users is an important issue in networks<sup>6</sup>. The multiaccess function is defined as the media access control (MAC) sublayer in the data link layer<sup>5</sup>. In this dissertation, a new MAC protocol suitable for wireless LANs is designed and analysed<sup>7</sup>. The protocol design is aimed at optimum utilisation of the radio channel by the users. The proposed protocol, called the optimum channel utilisation multiaccess (OCUM) protocol, is a hybrid protocol employing the *slotted ALOHA* and *busy tone sensing* concepts.

In slotted ALOHA, the overlapping transmissions from uncoordinated users result in low channel efficiency and the maximum achievable throughput is limited to 0.368. Carrier-sensing protocols like CSMA can achieve throughputs as high as 0.7 through more coordination among the users by sensing the state of the data channel (busy or idle) before transmission. However, carrier-sensing protocols degrade in performance when the propagation delay is not small compared to the packet transmission time. Also, carrier sensing when applied to wireless

networks suffers severe performance degradation due to *hidden node problem*. Busy tone access (BTMA) schemes have been proposed and studied to alleviate these problems. In our protocol design, we combine the advantage of slotted systems and busy tone sensing to overcome the above problems encountered in carrier-sensing protocols.

We show that by adopting a *preamble transmission policy* at the source node prior to the transmission of the actual data packets and a *busy tone broadcast policy* initiated by the destination node, the OCUM protocol fully overcomes the problem of hidden node and offers throughputs as high as 1.0 with multiple data packets per message.

We present the throughput and delay performance of the OCUM protocol estimated through analysis and simulation for various network conditions like different types of network traffic, capture effect, finite buffer capacity at each node, dual channel operation, high speed and multihop environments.

## 2. OCUM protocol description

The proposed OCUM protocol<sup>7</sup> uses two independent radio channels, namely, *Message channel* (M-channel) and *Busy tone channel* (B-channel). The M-channel is a high bandwidth channel used for the transmission of data packets and the B-channel is meant for carrying a narrowband busy tone to indicate the activity on the M-channel. The presence or absence of the busy tone on B-channel indicates whether the M-channel is busy or idle. The M-channel is slotted to one data packet duration and transmission attempts are made at the slot boundaries. The protocol uses a control packet known as the *preamble packet* for each message. The preamble packet size is equal to one data packet size and it has the intended *destination node address* embedded into it. The busy tone is broadcast by the intended destination node while it successfully receives data packets from the source node.

The channel access mechanism of the OCUM protocol is such that a node having a message to transmit first senses the B-channel. If the busy tone is present on the B-channel, it refrains from making a transmission attempt and reschedules the transmission attempt to a later time. If the busy tone is absent, it makes the transmission attempt by sending the preamble packet, which contains the destination node address in its address field, on the M-channel and looks for the busy tone response from the destination node. If the preamble transmission gets through the channel without collision or channel errors, the preamble packet will be correctly received by all the nodes which are in the connectivity range and line-of-sight of the source node. However, only the intended destination node acknowledges the preamble and broadcasts the busy tone. On hearing the busy tone response, the source node transmits the data packets continuously on the M-channel until the entire message is sent. The destination node terminates the busy tone broadcast once the message reception is complete. However, if the preamble packet is lost (or corrupted) due to collision or channel errors, the sender node will not receive the busy tone response and the transmission attempt is rescheduled to a later time.

It may be seen that in the OCUM protocol described above, preamble transmission policy is governed by the slotted ALOHA protocol coupled with the busy tone sensing on the B-channel. Also, the busy tone broadcast serves two purposes, viz., 1. it serves as the preamble acknowledgement mechanism, and 2. it inhibits all the neighbouring nodes of the intended destination (other than the source node) from interfering with the data packets reception, thus avoiding the hidden node problem.

By restricting the collision to occur only among preamble packets rather than data packets the utilisation of the M-channel becomes effective.

### 2.1. Throughput performance

The throughput performance of the OCUM protocol for a fully connected wireless LAN is studied through *Markov chain analysis*. Initially, two types of network traffic having different arrival processes are considered. They are *Bernoulli* arrival process at each node in a *finite population* network model and *Poisson* arrival process in an *infinite population* network model. In both the cases, all nodes are assumed to be *homogeneous* having *no buffers* and the rescheduled messages are assumed to be regenerated fresh. The propagation and processing delays are assumed to be negligible compared to the packet duration which implies *instantaneous busy tone feedback* for the preamble success event. A collision is said to occur if more than one node transmit preamble packets dur-

ing the same slot. The M-channel is assumed to be error free and packet losses, if any, are only due to collision. The message lengths are assumed to follow *geometric* distribution. Expressions for the M-channel throughput, idle rate and collision rate are derived for the analytical model considered above. The throughput expression for the Bernoulli arrival process is shown to be

$$\eta_{ber} = \frac{(1 + g_m) N \lambda (1 - \lambda)^{N-1}}{g_m + N \lambda (1 - \lambda)^{N-1}}$$

where  $N$  is the number of nodes in the network,  $\lambda$ , the Bernoulli message arrival rate at each node and  $g_m$ , the parameter of the geometric distribution of message length ( $0 < g_m < 1$ ).

For Poisson arrival process with  $G$  message arrivals/slot offered load into the network, the throughput is derived as

$$\eta_{poi} = \frac{(1 + g_m) G e^{-G}}{g_m + G e^{-G}}$$

Numerical results show that the OCUM protocol offers good throughput performance with maximum channel utilization of the order of 0.78. Maximum throughput is shown to occur at  $\lambda = 1/N$  for Bernoulli arrival process. At arrival rates greater than  $1/N$  the collision rate increases resulting in system instability with degraded throughput performance. For Poisson arrival process, the maximum throughput is shown to occur at  $G = 1$ . It is found that the channel utilisation is further improved for larger message sizes which make the OCUM protocol suitable for file transfer type of applications.

## 2.2. Capture effect

In the throughput analysis presented above, it has been assumed that collision between more than one preamble packet results in irrecoverable destruction of the packets involved. This assumption is overly pessimistic for wireless LANs since it does not consider the *effect of capture* in radio channels. Capture effect is a phenomenon unique to radio channels by which a discrepancy in the received power between two or more overlapping signals allows the receiver to correctly receive the strongest one. Clearly, capture effect improves the system performance and by adopting adaptive power control it allows one to achieve either fairness to all nodes or selective discrimination. In this dissertation, the effect of capture on the throughput performance of the OCUM protocol is studied under three different multiple transmit power level (MTPL) schemes<sup>8,9</sup>.

In MTPL Schemes I and II, each node has two different transmit power levels,  $\{P_T, YP_T\}$ , on the M-channel. Scheme I proposes allocation of implicit priority to the nodes by dividing the network population into two classes of nodes based on the signal strength (power) with which they transmit on the M-channel. High-power (Class-H) nodes get higher priority over low-power nodes (Class-L) due to capture phenomenon. In Scheme II, all the nodes are homogeneous with each node having the capability to transmit either with high or low power, the selection of which is done through a random probabilistic rule that ensures fairness to all nodes. In MTPL Scheme III, all the nodes have the capability to transmit with any one of  $m$  ( $m \geq 2$ ) linearly spaced transmit power levels employing random power level selection. Though Scheme II can be treated as a special case of Scheme III for  $m = 2$ , it is separately considered to study the effect of the magnitude of separation between the high and low transmit power levels.

The Markov chain analyses of the above three schemes for *infinite population network* with *Poisson arrivals* are carried out to estimate the throughput performance. The assumptions made earlier regarding no buffer, error-free M-channel, instantaneous busy tone feedback and geometric distribution of message length are made here. The throughput expression for Scheme I has been derived as

$$\eta = \frac{(1 + g_m) \left[ p_{0h} p_{1l} + p_{1h} \sum_{k=0}^{C_T} p_{kl} \right]}{g_m + p_{0h} p_{1l} + p_{1h} \sum_{k=0}^{C_T} p_{kl}} \quad (\text{Scheme I})$$

where  $p_{kh}$  and  $p_{kl}$  are the probabilities that  $k$  ( $=0, 1, 2, 3, \dots$ ) number of class-H and -L nodes get message arrivals in a slot and  $C_T = (Y-1)$  is the *capture threshold*. The throughput expression for Scheme II is derived as

$$\eta = \frac{(1 + g_m) \left[ Ge^{-G} + \sum_{k=2}^Y \frac{G^k e^{-G}}{(k-1)!} (1-p_l) p_l^{k-1} \right]}{g_m + Ge^{-G} + \sum_{k=2}^Y \frac{G^k e^{-G}}{(k-1)!} (1-p_l) p_l^{k-1}} \quad (\text{Scheme II})$$

$p_l$  and  $p_h$  are the probabilities of choosing the high or low transmit power levels such that  $p_h = (1-p_l)$ . For MTPL Scheme III, the throughput expression is derived as

$$\eta = \frac{(1 + g_m) \left[ \sum_{k=1}^m \frac{G^k e^{-G}}{k!} k \left( \frac{1}{m} \right)^k m_{c_k} \right]}{g_m + \sum_{k=1}^m \frac{G^k e^{-G}}{k!} k \left( \frac{1}{m} \right)^k m_{c_k}} \quad (\text{Scheme III})$$

where  $m$  is the number of available transmit power levels at each node.

Numerical results show improvement in the OCUM protocol throughput of the order of 0.9 due to capture effect in all the three schemes. It is shown that a capture threshold of  $C_T = 3$  achieves throughput as close as the theoretical upper bound corresponding to infinite capture threshold. Also the throughput improvement in Scheme III tends to get saturated for  $m > 6$ .

### 2.3. Finite buffer capacity at each node

For the regenerative traffic model assumed under no buffer conditions in the above analyses, the results show that like in any other random access protocol, the OCUM protocol also shows unstable behaviour when the offered load is high. This unstable behaviour is controlled by considering *finite buffer capacity* ( $L$ ) at each node and enforcing a *message reject policy* which discards all new messages arriving at the nodes when the message buffers are full. Estimating the protocol performance through exact analysis under such conditions tends to be complex because the number of states that describe the system increases as the number of message buffers at each node is increased. Hence, approximate analytical methods or simulation techniques are often adopted. In this dissertation, we adopt the simulation approach and estimate the throughput and delay performance of the OCUM protocol under finite buffer conditions.

The simulation model of the finite buffer OCUM protocol considers a *finite population*, fully connected network with *homogeneous* nodes. The buffer capacity at each node is finite ( $\geq 1$ ) and each buffer can hold one message. New message arrivals follow Bernoulli process. Rescheduled messages are retained in the buffer until they are successfully sent to the destination. The retransmission delay distribution is considered to be geometrically distributed. Performance measures like M-channel throughput and average message transfer delay are estimated. Simulation results show that the protocol offers constant throughput of the order of 0.8–0.9 at high arrival rates. The throughput is found to improve at low arrival rates when the value of  $L$  is increased. However, the throughput improvement becomes marginal for  $L > 4$ . Near 100% channel utilisation is achieved at the cost of increased message transfer delays.

### 2.4. Dual channel operation

The capacity of a wireless LAN can be increased by two approaches, namely, (a) adding additional message channels at the same data rate, and (b) by increasing the data rate of a single message channel. In this dissertation, both the approaches are investigated for the OCUM protocol.

We study the dual channel operation of the OCUM protocol (DC-OCUM)<sup>10</sup> which uses two independent message and busy tone channel pairs. The throughput performance of the DC-OCUM protocol has been estimated for fully connected network with finite buffers at each node through simulation. The channel selection mechanism is an important issue in the dual channel operation. Two types of *channel selection policies* for making a transmis-

sion attempt are studied and compared. In the first channel select policy, sensing of all channels is performed first and a channel is chosen randomly from the available idle channels. In the second policy, any one of the channels is selected randomly first and then the chosen channel is sensed for making a transmission attempt. It is shown that the first policy performs better than the second.

### 2.5. High-speed channel environment

For a single high-speed M-channel scenario, the OCUM protocol needs to be modified to take care of the effects of propagation and processing delays which become comparable or greater than the packet duration. The modified OCUM (MOCUM)<sup>11</sup> protocol and its throughput performance for fully connected network with no buffers at the nodes are presented. Simulation results show that while the propagation and processing delays degrade the throughput increasingly with the delay constant (a factor equal to the smallest integer greater than or equal to the ratio between the two-way radio propagation and processing delays to the packet duration), the protocol is still found to offer throughputs of the order of 0.4–0.7 for wireless LANs up to 100 Mbps rate and 10 km range.

### 2.6. Multihop environment

The throughput and delay performance of the OCUM protocol in a *multihop* environment are studied through simulation. Partially connected static topologies with finite number of nodes that are globally synchronised to the slot duration are considered. Each node has unlimited buffer resources for *transmitting messages* and limited buffer capacity for new *entry messages*. An input buffer limiting (IBL) policy rejects entry of new messages into a node when the total number of queued up messages (including entry and transit messages) exceeds a specific threshold. The entry and transit messages at each node are given a first-come-first served (FCFS) service discipline. The routing algorithm used is a *static shortest path scheme*. Simulation results for specific topologies like ring, bus, square lattice, multiconnected ring and other arbitrary topologies are presented. It is shown that throughputs of the order 1.0–1.8 are achieved for  $N = 5$  with different topologies. Such increased throughputs are realised due to *spatial reuse* in multihop operation.

### 2.7. Scope for further study

Further to the design and performance results presented in this dissertation, there is scope for future extensions to the work. We have assumed error-free M-channel without fading and multipath throughout. The effect of channel errors, fading and multipath on the OCUM protocol performance both in indoor and outdoor wireless environments can be studied. The effect of capture and finite buffer capacity in multihop networks can be considered for high-speed wireless networks operating with modified OCUM protocol. In the multichannel environment, we have studied only the dual channel operation. The study of a more generalised  $n$ -channel ( $n > 2$ ) system is another potential area of future work. Other possible extensions will be the study of OCUM protocol performance under dynamic topology variations due to node and link failures in the presence of mobile users in the network.

## References

1. ACAMPORA, A. S. AND WINTERS, J. H. A wireless network for wide-band indoor communications, *IEEE J.*, 1987, SAC-5, 796–805.
2. BUCHHOLZ, D., ODLYZKO, P., TAYLOR, M. AND WHITE, R. Wireless in-building network architecture and protocols, *IEEE Network Mag.*, 1991, 5, 31–38.
3. LYNCH, C. A. AND BROWNRIGG, E. B. *Packet radio network—Architecture, protocols, technologies and applications*, 1987, Pergamon Press.
4. RAPPAPORT, T. S. Indoor radio communications for factories of the future, *IEEE Commun. Mag.*, 1989, 27, 15–24.
5. LI, V. O. K. Performance evaluation of multiple-access network: Introduction and overview, *IEEE J.*, 1987, SAC-5, 933–937.

6. RUBIN, I. AND BAKER, J. E. Media access control for high-speed local area and metropolitan area communications networks, *Proc. IEEE*, 1990, 78, 168-203.
7. CHOCKALINGAM, A., VENKATARAM, P. AND PRABHAKAR, A. Design of an optimum channel utilisation multiaccess protocol for packet radio networks, *J. Instn Elect. Telecom. Engrs*, 1992, 38, 334-343.
8. CHOCKALINGAM, A., VENKATARAM, P. AND PRABHAKAR, A. Throughput analysis of a class of multiaccess protocol for packet radio networks with capture effect, *Proc. Singapore Int. Conf. on Networks (SICON)*, pp. 376-381, September 1991.
9. CHOCKALINGAM, A., VENKATARAM, P. AND PRABHAKAR, A. Multiple transmit power level schemes in wireless LANs: MAC layer performance, submitted to *IEEE/ACM Trans. Networking*.
10. CHOCKALINGAM, A., VENKATARAM, P. AND PRABHAKAR, A. Dual channel OCUM protocol for wireless LANs, *IEEE Int. Conf. on Sel. Topics in Wireless Commun.*, Vancouver, B. C., Canada, June 1992.
11. CHOCKALINGAM, A., VENKATARAM P. AND PRABHAKAR, A. Effect of propagation and processing delays on the throughput performance of a class of multiaccess protocol for high speed radio LANs, *Proc. IEEE GLOBECOM*, Vol. 2, pp. 906-910, Phoenix AZ, December 1991.

### Thesis Abstract (Ph. D.)

## Reliability and performability analysis of distributed memory multicomputers by Samir Mahmoud Koriem

Research supervisor: L. M. Patnaik

Department: Computer Science and Automation

### 1. Introduction

Conventionally, fault-tolerant computer systems have been evaluated in terms of performance and reliability. Evaluating both performance and reliability is essential for the characterization and design of any system. However, neither performance nor reliability *alone* can completely characterize the behavior of a gracefully degradable system. Hence, an approach for combining both performance and reliability, called performability<sup>1</sup>, is needed to assess the effectiveness of a computer system. The performability studies try to answer the question of how well a system works even when the computing power is reduced. In this context, we propose a modeling framework<sup>2</sup> that allows an easy, efficient, and accurate evaluation of fault-tolerant multicomputer systems. The specific problems addressed are reliability, performance, and the combination of reliability and performance analysis of distributed memory multicomputer systems. Based on the use of generalized stochastic Petri net<sup>3</sup> (GSPN) approach, our framework is able to model various aspects of distributed system behavior such as concurrency, synchronization, contention, and graceful degradation.

While it is important to model and analyze the composite performance and reliability of multicomputer systems (networks) for achieving good system design, efficient interprocessor communication is a key parameter to achieve high performance in these systems. Thus, modeling and analyzing message communication latency is critical for optimizing the performance of interprocessor communication. In order to demonstrate how to achieve efficient (low latency) interprocessor communication, we have developed GSPN routing models for hypercube and mesh networks that employ either *message switching*, *packet switching*, or *warmhole switching* techniques. These GSPN routing models have also been used to describe the following interesting communication patterns occurring in hypercube and mesh networks: (i) *congestion-free* adjacent and non-adjacent node communication patterns; and (ii) adjacent and non-adjacent node *congestion*<sup>4</sup> communication patterns.

Throughout our performance, reliability or performability analysis of distributed memory multicomputer systems, we have used GSPN since it is a powerful and flexible modeling tool. From our practical use of the GSPN technique, we find that the Markov chains derived from the GSPN model suffer from the problem of exponential state space explosion. In order to try to tackle this problem, we propose a *generalized stochastic high-level Petri net*<sup>1</sup> (GSHLPN) as a modeling technique for evaluating the performance of parallel and distributed systems.

## 2. Modeling performability

A major objective of our research work is the development of a novel modeling technique based on GSPN approach to study and analyze the hypercube reliability, and also to study the effects of reliability on the performance and reliability (*performability*) based on the GSPN technique.

In our GSPN performance models, important aspects of hypercube architecture such as concurrency, message passing mechanism between the host and the nodes as well as among the nodes, have been modeled in a natural way. The capability to model such diverse aspects of system behavior has been illustrated through modeling the execution of four realistic parallel algorithms on an iPSC/2 hypercube. These four representative parallel algorithms have been chosen to be two matrix multiplication algorithms, a bitonic sort algorithm, and a quicksort algorithm. We have carried out a mathematical analysis of the four algorithms to verify the correctness of the result obtained from the GSPN performance models.

A novelty of our reliability analysis of hypercube architecture is that we have developed simple GSPN reliability models that give all the features of the *subcube reliability approach* and *disconnected reliability approach* in an elegant way. Also, to obtain realistic reliability results, we have included the *coverage* and *repair* strategies in our GSPN reliability models. The main advantages of our GSPN reliability models over the subcube and disconnected reliability approaches can be summarized as follows. In our GSPN reliability models, the number of places and transitions can only marginally increase as the complexity of the modeled hypercube system increases, while the number of states in the Markov chain of the subcube and disconnected reliability approaches increases exponentially. Since the Markov chain is automatically generated from the GSPN model, we do not have to manually enumerate all the possible states of the Markov chain unlike the subcube and disconnected reliability approaches. Furthermore, our GSPN reliability technique does not require a closed-form solution unlike the subcube and disconnected reliability approaches.

In order to assess the effectiveness of hypercube multicomputer systems, *performability models* that combine reliability models and performance metrics have been studied<sup>2</sup>. Using the *GSPN-reward* technique<sup>1</sup>, the performability model is built by evaluating the performance metrics (*e.g.*, the mean time to complete the program) for each state of the Markov reliability model. The performability model is analyzed to obtain various *instantaneous* and *cumulative measures*. Furthermore, our study indicates how changes in the *performability* model parameters of the hypercube system such as the node failure rate, repair strategy, and coverage strategy affect the performability metrics (*e.g.*, expected reward rate, and expected accumulated reward). This *sensitivity analysis* is a useful technique to identify the performability model parameters that are likely to produce significant modeling errors.

## 3. Modeling message routing

An important contribution of this thesis is the development of *easy, efficient, and accurate GSPN routing models* for studying the communication behavior of hypercube and mesh multicomputer networks that use either message switching, packet switching, or wormhole switching techniques. The novelty of our GSPN routing models is that they can represent the following communication patterns occurring in hypercube and mesh networks.

1. Under *congestion-free adjacent node communication patterns*, we have developed both GSPN and mathematical routing models. The results obtained from the mathematical models have been used to verify the correctness of the results obtained from the analysis of the GSPN routing models.

2. Under *congestion-free non-adjacent communication patterns*, we have developed GSPN routing models for hypercube and mesh multicomputer networks. We have considered *message switching, packet switching, and wormhole switching techniques* as the basic underlying communication mechanisms of these networks. In the developed models, both wormhole and packet switched networks have been analyzed under *parallel path trans-*

*mission* and *pipeline transmission* methods. We have also developed the corresponding mathematical models. These mathematical routing models have been used to validate the numerical results obtained from the GSPN models.

3. Under *congestion communication patterns*, we have developed GSPN routing models to examine the effects of congestion problems such as *buffer overflow* and *channel contention* on the communication latency to messages in multicomputer networks<sup>4</sup>. In these models, the behavior of the buffers and the communication channels is characterized by the range of *blocking probability* and *contention probability* values, respectively. In order to provide practical insights into the operation of actual multicomputer networks under these congestion problems, we have incorporated the basic features of the *routing control mechanisms* into our GSPN routing models.

Our GSPN routing models were shown to be able to satisfactorily describe and analyze the following communication aspects: (i) the *congestion* among arriving messages at *each node/link*; and (ii) the behavior of transmitting a message from the source node to the destination node through the *multihops* that a message must travel. Such communication aspects are difficult to model and numerically solve by using queueing network approach. A comprehensive treatment on the use of GSPN methods has been presented, which is also intended to be useful for solving many other related network problems such as fault-tolerant communication.

#### 4. GSHLPN technique

Although GSPN represents a powerful and flexible modeling tool, the Markov chains derived from the GSPN models suffer from the problem of exponential state space explosion. In order to try to solve this problem, we have proposed a GSHLPN<sup>5</sup> as a modeling technique for evaluating the performance of parallel and distributed systems. This developed model is a hybrid of the *predicate/transition net* (PrT-net) and the *generalized stochastic Petri net* (GSPN).

We have also defined a method for performance analysis of the GSHLPN model incorporating the *compound marking technique*. An important advantage of this method is the reduction in the state space size of the GSHLPN model. A few illustrative examples have been analyzed using our models as well as the GSPN model, and the results have been discussed. A comparison of these results shows that the GSHLPN model indeed has smaller number of places, transitions, and states than those of the model constructed using GSPN for the same system. The GSHLPN model is especially useful for the analysis of complex systems due to its advantage of conciseness and simplicity. We have also discussed the application of our model to the performance analysis of the message-passing hypercube systems.

We have demonstrated how one can apply the *time scale decomposition technique* and the *compound marking technique* to the GSHLPN model. This application introduces an alternative method to further reduce the state space size of complex GSHLPN system models.

#### References

1. CIARDO, G., MUPPALA, J. AND TRIVEDI, K. On the solution of GSPN reward models, *Performance Evaluation*, 1991, 12, 237-253.
2. KORIEM, S. M. AND PATNAIK, L. M. Fault-tolerance analysis of hypercube systems using Petri nets theory, *J. Systems Software*, 1993, 21, 71-88.
3. MARSON, M. A., BALBO, G. AND CONTE, G. A class of generalized stochastic Petri nets for the performance evaluation of multiprocessor systems, *ACM Trans. Computer Systems*, 1984, 2, 93-122.
4. KORIEM, S. M. AND PATNAIK, L. M. Performance of the node/link behavior of multicomputer networks with input buffer limiting and channel contention, *Computer Commun.*, 1994, 17, 647-656.
5. KORIEM, S. M. AND PATNAIK, L. M. Performance evaluation of distributed memory architectures using generalized stochastic high-level Petri nets, *Al-Azhar Engng Second Int. Conf.*, Cairo, Egypt, Dec, 1991, pp. 37-48.

Thesis Abstract (Ph. D.)

Determining and connecting all the extrema of a function over a compact manifold

by H. Shashikala

Research supervisor: S. Sathiya Keerthi

Department: Computer Science and Automation

### 1. Introduction

In this thesis we give a method for determining and connecting all the local minima and local maxima of a function on a compact manifold. Let  $C^2$  denote the set of functions from  $R^n \rightarrow R$  whose derivatives up to second order are continuous. Given  $f$  and  $h_i, i = 1, \dots, m$ , to be functions in  $C^2$ , define

$$\tilde{\Omega} = \{x \in R^n : h_i(x) = 0, i = 1, \dots, m\}. \quad (1)$$

Assume that  $\tilde{\Omega}$  is a compact differentiable manifold. Let  $x^* \in \tilde{\Omega}$  be given. We consider the problem of connecting all the local minima and local maxima of  $f$  on the set  $\Omega \subset \tilde{\Omega}$  defined by

$$\Omega = \text{the connected component of } \tilde{\Omega} \text{ containing } x^*. \quad (2)$$

Clearly,  $\Omega$  is a connected, compact differentiable manifold. Further,  $\Omega = \tilde{\Omega}$ , if  $\tilde{\Omega}$  is connected.

DEFINITION 1. Consider

$$X = \{x \in R^n : h_i(x) = 0, i = 1, \dots, m, g_j(x) \leq 0, j = 1, \dots, l\}, \quad (3)$$

where  $h_i, g_j \in C^2$ . Let  $x \in X$  and  $J = \{j : g_j(x) = 0\}$ .  $\bar{x}$  is said to be *regular* if the set of gradients  $\{\nabla h_i(\bar{x}), i = 1, \dots, m\} \cup \{\nabla g_j(\bar{x}) : j \in J\}$  is linearly independent.

ASSUMPTION  $A_1$ . All  $x \in \Omega$  are regular.

The above assumption is generically true. Define the Lagrangian  $L : R^n \times R^m \rightarrow R$  of  $f$  over  $\Omega$  as  $L(x, \lambda) = f(x) + \sum_{i=1}^m \lambda_i h_i(x)$ . A point  $\bar{x} \in \Omega$  is said to be a *critical point of  $f$  over  $\Omega$*  if  $\exists \lambda \in R^m$  such that

$$\nabla_x L(\bar{x}, \bar{\lambda}) = \left( \frac{\partial L}{\partial x_1}(\bar{x}, \bar{\lambda}), \dots, \frac{\partial L}{\partial x_n}(\bar{x}, \bar{\lambda}) \right)^T = 0,$$

where  $T$  denotes transpose. By Assumption  $A_1$ , the  $\bar{\lambda}$  associated with  $\bar{x}$  is unique.

Let  $Z$  denote the set of all critical points of  $f$  over  $\Omega$ ; and,  $MIN$  and  $MAX$  represent the set of all local minima and local maxima of  $f$  over  $\Omega$ , respectively. Assumption  $A_1$  allows Lagrange multiplier rule to be used and so we get  $MIN \cup MAX \subset Z$ .  $SAD = Z \setminus (MIN \cup MAX)$  is the set of all saddle points.

There is some literature on related problems. Special homotopy methods for determining all critical points of a polynomial system are well known<sup>1</sup>. However, these methods have practical value only if the degree of the system is small. Also the extension of the homotopies to general nonlinear systems is unclear. Further, the homotopy curve is in the complex domain and may consist of several components; thus, it may not be helpful in connecting all the critical points. Deiner<sup>2</sup> uses a homotopy formulation and gives a recursive construction that yields a one-dimensional web containing all the critical points. But he needs an algorithm to find all the roots of a system of nonlinear equations. Thus, it is not of much practical value. Canny<sup>3</sup> has given a provably correct algorithm to connect all the critical points of a polynomial over a semi-algebraic set. Apart from its restriction to problems with algebraic description, Canny's method is difficult to implement and has not been proven to be practically useful. Branin<sup>4</sup> tries to get a single trajectory connecting all the critical points by alternately maximizing and minimizing the function. Treccani<sup>5</sup> gives a counterexample where Branin's method fails.

In our approach, we form a directed graph  $G$  with all the local minima and local maxima as its vertices.  $G$  is a bipartite graph with  $MIN$  and  $MAX$  as partitions. An edge connecting  $x_i$  to  $x_j$  has an associated weight vector which encodes a way of connecting  $x_i$  to  $x_j$  via a continuous path on  $\Omega$ .

## 2. Our method

We begin with some definitions. Let  $\Omega$  be as defined by (2). For  $\bar{x} \in \Omega$ , denote the tangent space of  $\Omega$  at  $\bar{x}$  by  $T_{\bar{x}}(\Omega)$ .

**DEFINITION 2.** Consider  $x^*$ , a critical point of  $f$  over  $\Omega$ . Let  $\lambda^*$  denote the Lagrangian multiplier vector associated with  $x^*$ ;  $\nabla_x^2 L(x^*, \lambda^*)$  denote the Hessian of  $L$  with respect to  $x$  at  $x^*$ ;  $B$  be an  $n \times (n - m)$  matrix whose columns form an orthogonal basis for  $T_{x^*}(\Omega)$ ;  $H = B^T \nabla_x^2 L(x^*, \lambda^*) B$ ; and  $\alpha_1, \dots, \alpha_{n-m}$  be the eigenvalues of  $H$ . We say that  $x^*$  is a *hyperbolic critical point* if  $\alpha_i \neq 0, i = 1, \dots, (n - m)$ .

**ASSUMPTION  $A_2$ .** All critical points of  $f$  over  $\Omega$  are hyperbolic.

The above assumption holds generically<sup>6</sup>. By compactness of  $\Omega$ , there will only be a finite number of hyperbolic critical points of  $f$  over  $\Omega$ <sup>7</sup>. Two differentiable manifolds  $A$  and  $B$  in  $\Omega$  are said to be *transversal* if either  $T_x(A) + T_x(B) = T_x(\Omega) \forall x \in A \cap B$ , or  $A \cap B = \phi$ .

Let  $\dot{x} = dx/dt$  and consider the following differential-algebraic systems (in  $x$  and  $\lambda$ ):

$$\dot{x} = -\nabla_x L(x, \lambda), \quad \langle \nabla h_i, \dot{x} \rangle = 0, \quad i = 1, \dots, m; \quad (4)$$

$$\dot{x} = \nabla_x L(x, \lambda), \quad \langle \nabla h_i, \dot{x} \rangle = 0, \quad i = 1, \dots, m. \quad (5)$$

These systems denote the vector fields in which  $\dot{x}$  is the projection of  $-\nabla f(x)$  and  $\nabla f(x)$  on to  $T_x(\Omega)$ . Given  $x_0 \in \Omega$ , let  $\Phi^-(t, x_0)$  and  $\Phi^+(t, x_0)$  denote the solutions of (4) and (5), respectively, with  $x(0) = x_0$ . All solutions of (4) and (5) which start in  $\Omega$  will remain in  $\Omega$  and asymptotically reach one of the critical points of  $f$  over  $\Omega$ <sup>8</sup>.

Let  $\bar{x}$  be a critical point of  $f$  over  $\Omega$ . Define,

$$W^-(\bar{x}) = \{x \in \Omega : \lim_{t \rightarrow \infty} \Phi^-(t, x) = \bar{x}\}, \text{ and } W^+(\bar{x}) = \{x \in \Omega : \lim_{t \rightarrow \infty} \Phi^+(t, x) = \bar{x}\}.$$

If  $\bar{x} \in MIN$ , then  $W^-(\bar{x})$  denotes the region of attraction of  $\bar{x}$ . Similarly, if  $\bar{x} \in MAX$ , then  $W^+(\bar{x})$  is the region of attraction of  $\bar{x}$ .

**ASSUMPTION  $A_3$ .**  $W^-(\bar{x})$  and  $W^-(\bar{y})$  intersect transversally for all  $\bar{x}, \bar{y} \in Z$ .

Assumption  $A_3$  is also generic<sup>8</sup>. Given  $x \in R^n$  and  $\epsilon > 0$ , let  $B_\epsilon(x) = \{z : \|z - x\| < \epsilon\}$ , where  $\|\cdot\|$  denotes the Euclidean norm in  $R^n$ . We define a local maximum  $y$  to be *adjacent* to a local minimum  $x$  if  $\forall \epsilon > 0 \exists z \in B_\epsilon(x)$  such that  $\lim_{t \rightarrow \infty} \Phi^+(t, z) = y$ . Similarly, a local minimum  $x$  is said to be *adjacent* to a local maximum  $y$  if  $\forall \epsilon > 0, \exists z \in B_\epsilon(y)$  such that  $\lim_{t \rightarrow \infty} \Phi^-(t, z) = x$ . With  $x$  and  $y$  as given above, it is easy to see that  $y$  is adjacent to  $x$  if  $x$  is adjacent to  $y$ . Hence we can simply talk in terms of  $x$  and  $y$  being adjacent. As stated before, our aim is to connect all the local maxima and local minima of  $f$  over  $\Omega$ . We form a directed graph  $G$  as follows. The set of vertices of  $G$  is  $MIN \cup MAX$ . An edge is connected from vertex  $x$  to vertex  $y$  if  $x$  and  $y$  are adjacent. The following theorem is proved<sup>9</sup>. The proof uses the results in Canny<sup>3</sup> strongly.

**THEOREM 1.** Suppose Assumptions  $A_1, A_2$  and  $A_3$  hold. Then  $G$  is connected.

Two important remarks should be made here. First, Theorem 1 may not hold if  $\Omega$  is not compact. Second, if we take  $Z$  as the set of vertices and define a corresponding graph  $\tilde{G}$  (an extension of  $G$ ) then Theorem 1 will hold if  $G$  is replaced by  $\tilde{G}$ . In fact, the proof of this modified theorem is much easier. We have chosen  $G$  instead of  $\tilde{G}$

because saddle points are difficult to reach, *i.e.*, only a set of measure zero starting points in  $\Omega$  will reach saddles under the flow defined by (4) or (5).

Consider the construction of  $G$ . Let  $x$  be a local minimum and  $y_1, \dots, y_l$  be the local maxima adjacent to  $x$ . We need an algorithm  $A^+$  which takes  $x$  as input and for any given  $\epsilon > 0$ , outputs  $y_i$  and perturbations  $p_i$  such that  $\|p_i\| \leq \epsilon$  and  $\lim_{t \rightarrow \infty} \Phi^+(t, x + p_i) = y_i$ , for  $i = 1, \dots, l$ . In other words,  $A^+$  connects a local minimum to all its adjacent local maxima. We also need an algorithm  $A^-$  which takes a local maximum as input and outputs all its adjacent local minima with the corresponding perturbations. An exact realization of  $A^+$  and  $A^-$  is hard. For practical implementation,  $A^+$  and  $A^-$  are replaced by heuristic approximations. Some powerful heuristics for the implementation of  $A^+$  and  $A^-$  are described in detail<sup>9</sup> and briefly sketched further below.

The construction of  $G$  is given by the following conceptual algorithm.

ALGORITHM FORM-GRAPH ( $x^*$ ) \ \* $x^* \in \Omega$  is a given point. \* \

- 1: Set  $V_1 = \phi$ ,  $V_2 = \phi$ ,  $E = \phi$ ,  $V = \phi$ . Choose a small  $\epsilon > 0$  for use in  $A^+$  and  $A^-$ .
- 2: Integrate (4) to find  $\bar{x} = \lim_{t \rightarrow \infty} \Phi^-(t, x^*)$ . Set:  $V_1 = \{\bar{x}\}$ ,  $V = \{\bar{x}\}$
- 3: While ( $V \neq \phi$ ) do

Begin

Pick  $x \in V$ . Set  $V = V \setminus \{x\}$ .

If  $x \in MIN$ , apply  $A^+$  to find all its adjacent local maxima  $y_1, \dots, y_l$  and corresponding perturbations  $p_1, \dots, p_l$  such that  $\lim_{t \rightarrow \infty} \Phi^+(t, x + p_i) = y_i$ ,  $i = 1, \dots, l$ ,  $\|p_i\| < \epsilon$ . Set  $V = V \cup \{y_1, \dots, y_l\} \setminus V_2$ ;

$V_2 = V_2 \cup \{y_1, \dots, y_l\}$ ; and,  $E = E \cup \{(x, y_1, p_1, 1), \dots, (x, y_l, p_l, 1)\}$ .

Else

If  $x \in MAX$ , apply  $A^-$  to find all the adjacent local minima  $z_1, \dots, z_r$ , and corresponding perturbations  $q_1, \dots, q_r$  such that  $\lim_{t \rightarrow \infty} \Phi^-(t, x + q_i) = z_i$ ,  $i = 1, \dots, r$ ,  $\|q_i\| < \epsilon$ . Set  $V = V \cup \{z_1, \dots, z_r\} \setminus V_1$ ;

$V_1 = V_1 \cup \{z_1, \dots, z_r\}$ ; and,  $E = E \cup \{(x, z_1, q_1, -1), \dots, (x, z_r, q_r, -1)\}$ .

End.

At the end of the above procedure we get two partitions of vertices  $V_1$  and  $V_2$  and an edge-list,  $E$ . With probability one we can say that the  $\bar{x}$  determined in step 2 is a local minimum<sup>8</sup>. By Theorem 1, the graph determined by  $V_1$ ,  $V_2$  and  $E$  is the same as  $G$ . Thus,  $V_1$  is the set of local minima and  $V_2$ , the set of local maxima of  $f$  over  $\Omega$ . Each  $e \in E$  is of the form  $e = (x, y, p, s)$ .  $s = 1$  implies that  $x$  is a local minimum,  $y$ , a local maximum and  $\lim_{t \rightarrow \infty} \Phi^+(t, x + p) = y$ . Similarly,  $s = -1$  implies that  $x$  is a local maximum,  $y$ , a local minimum, and  $\lim_{t \rightarrow \infty} \Phi^-(t, x + p) = y$ .

Now, we briefly give the ideas behind three heuristics for the implementation of  $A^-$ . The ideas for  $A^+$  are similar. Let  $x^* \in MAX$ . The aim is to determine a set of 'small' perturbation vectors with the property that the solutions of (4), starting from the initial conditions generated by applying these perturbations on  $x^*$ , will lead to the set of all adjacent local minimizers of  $x^*$ . Since a solution of (4) is a solution of (5) with

Let  $\alpha_k$  denote the largest element of  $\{\alpha_i\}$  ( $\alpha_k$  is the element nearest to zero). It can be shown<sup>6</sup> that only a set of measure zero initial conditions in  $W^*(x^*)$  lead to solutions of (5) which approach  $x^*$  along axes other than  $v_k$ . Thus, we get the *dominating eigen-axis heuristic*: concentrate the choice of perturbation vectors around the direction,  $v_k$ . One way of implementing this heuristic is as follows. Let  $C^+$  denote the cone in  $T_{x^*}(\Omega)$  with apex at  $x^*$ , apex angle =  $\theta$  (a small amount, say 5 degrees) and axis along  $v_k$ ;  $C^-$  denote the symmetrically opposite cone at  $x^*$  with axis along  $-v_k$ ; and NTOL be a positive integer, say NTOL = 3 (larger the NTOL, better the heuristic but more is the computational effort). Choose the perturbation vectors from  $C^+$  and  $C^-$  randomly with a uniform distribution until NTOL consecutive perturbations fail to yield a new minimizer.

In the above heuristics, if perturbations are not chosen carefully along the eigen axes, the solutions of (4) can go to saddle points. So it may be useful to try perturbations away from the eigen axes. The third heuristic, called as *eigen-orthant heuristic*, is based on this observation. We choose one perturbation vector from the interior of each of the  $2^{n-m}$  orthants of the coordinate system for  $T_{x^*}(\Omega)$  formed by  $v_1, \dots, v_{n-m}$ . If  $(n-m)$  is large then this heuristic is not suitable and it can be replaced by a modification.

In numerical experiments we have found the dominating eigen-axis heuristic to be the most effective. We also note that, saddle points are encountered when the above heuristics are used. However, there is no harm in including them in an extended graph of the extrema.

### 3. Applications

In this section, we briefly describe three very useful problems which can be solved using our method. When applying our method, we will assume that the generic assumptions  $A_1$ ,  $A_2$ , and  $A_3$  always hold.

#### 3.1. Constrained global optimization

Consider the global solution of

$$\min f(x) \text{ s.t. } x \in X \quad (6)$$

where  $f \in C^2$  and  $X$  is as given by (3). Assume  $X$  is compact and connected and,  $\forall x \in X$ ,  $x$  is a regular point. Suppose  $x^0 \in X$  is given. To solve (6) using the ideas of Section 2, we introduce new variables  $z = (z_1, \dots, z_l)$  and define,

$$\Omega = \{(x, z) : x \in R^n, z \in R^l, h_i(x) = 0, i = 1, \dots, m, g_j(x) + z_j^2 = 0, j = 1, \dots, l\}.$$

It is easy to verify that  $\Omega$  is a smooth connected compact manifold and that,  $\forall (x, z) \in \Omega$ ,  $(x, z)$  is a regular point. Now we set  $z_j^0 = \sqrt{-g_j(x^0)}$  and use form-graph  $(x^0, z^0)$  to get the set of all the local minima and local maxima of (6). This set contains all the global minima and global maxima. Suppose the unconstrained global minimum of a function  $f$  is to be found and it is known to exist. This problem can be tackled by choosing a large radius  $R$ , setting  $X = \{x : \|x\|^2 \leq R^2\}$  and solving (6). The problem of finding all the roots of a system of nonlinear equations can be easily converted to an optimization problem and the method can be readily applied.

#### 3.2. Collision-avoidance path finding

The problem of planning a collision-free path for a robot in a workspace with obstacles can, with some approximation, be reduced to the motion of a point on a smooth compact manifold  $\tilde{\Omega}$  with a description of the form (1). Let  $x^*$  be a given point in  $\tilde{\Omega}$ . The path-finding problem consists of two parts: (i) given any  $x \in \tilde{\Omega}$ , determine if  $x \in \Omega$ , and (ii) if  $x \in \Omega$ , find a continuous path from  $x$  to  $x^*$ .

To solve this problem, we define a smooth potential function  $f: \tilde{\Omega} \rightarrow R$  such that  $f$  attains its global minimum at  $x^*$ . One such choice of  $f$  is given by  $f(x) = \|x - x^*\|^2$ . Use form-graph  $(x^*)$  to connect all the local minima and local maxima of  $f$  over  $\Omega$  by continuous trajectories described by the graph  $G$ . In general,  $f$  may have many more local minimizers in  $\Omega$  other than  $x^*$ . Given any  $x \in \tilde{\Omega}$ , find  $\bar{x} = \lim_{t \rightarrow \infty} \Phi^-(t, x)$ . With probability one we can say that,  $x \in \Omega$  iff  $\bar{x}$  is a vertex of  $G$ . If  $\bar{x}$  is not a vertex of  $G$ , we can conclude, with probability one, that

Let  $x \in \bar{D}$  be a vertex of  $G$ , use a suitable graph search algorithm on  $G$  to connect  $\bar{x}$  and  $x^*$ . This yields an

We have implemented the algorithm from-graph using the three heuristics for  $A^+$  and  $A^-$ . Several test problems from the application areas mentioned above have been successfully solved. Details on the efficiency of our method will be reported in a future paper.

#### References

1. **WILSON, A. P.** *Solving polynomial systems using continuation for engineering and scientific problems*, 1987, Prentice-Hall.
2. **DEWIL, L.** Trajectory nets connecting all critical points of a smooth function, *Math. Progm.*, 1986, 36, 340-352.
3. **CHAFFIN, L.** *The complexity of robot motion planning*, Ph.D. Dissertation, MIT, 1987.
4. **BRANIN, R. H.** A widely convergent method for finding multiple solution of simultaneous nonlinear equations, *IBM J. Res. Dev.*, 1972, 504-522.
5. **BRANIN, R. H.** On the convergence of Branin's method: A counter example. In *Towards global optimisation* (L. C. W. Dixon and G. F. Szego, eds), North-Holland/American Elsevier.
6. **PAUL, J. AND DE MELO, W. JR.** *Geometric theory of dynamical systems: An introduction*, 1981, Springer-Verlag.
7. **ROSENBLATT, V. AND POLLACK, A.** *Differential topology*, 1974, Prentice Hall.
8. **CHANG, H., HIRSCH, M. W. AND WILF, F.** Stability regions of nonlinear autonomous systems, *IEEE Trans.*, 1988, AC-33, 16-27.
9. **SUBRAMANIAM, H., SANCHETI, N. K. AND KANTH, S. S.** *An algorithm for connecting all the extrema of a function over a compact manifold: Theory and applications*, Technical Report 91-08, Department of Computer Science and Automation, Indian Institute of Science, Bangalore.

#### Thesis Abstract (Ph. D.)

**Studies in learning and representation in connectionist networks** by S. H. Srinivasan

Research supervisor: M. Narasimha Murty

Department: Computer Science and Automation

#### 1. Introduction

Neural networks consist of a large number of processing elements interacting through weighted connections to accomplish a particular task. The problem of finding the right interconnection strengths is the problem of learning. The type of modeling draws its inspiration from biological nervous systems and the perceptual and motor tasks accomplished by them.

Two of the major tasks attempted using neural networks are the *pattern association* and *content addressable memory (CAM)*. In pattern association, the task is the association between pairs of patterns. For example, the task of associating English and Greek alphabets (e.g.,  $a$  and  $\alpha$ ,  $b$  and  $\beta$ , etc.) is a pattern association task. The task of retrieving a prototype pattern from a corrupted or noisy description is a CAM task. These two tasks are respectively modeled as a function from one feature space to another and as a dynamical system in the feature space having the stored patterns as stable equilibrium points or attractors. Usually, feedforward network architec-

tures are used for pattern association and recurrent architectures for CAM. The major issues in feedforward networks are: learning rule and generalization. Those in CAMs are: capacity, number of spurious memories, sizes of basins of attractors, stability, etc.

One widely used learning rule for feedforward networks is the backpropagation rule<sup>1</sup>. Backpropagation rule is essentially an error minimization procedure coupled with an ordered way of computing derivative values so that only local information is used. One very popular model for content addressable memory is the Hopfield model<sup>2</sup>. In the present work, we raise certain questions relating to learning and representation in connectionist networks in the context of error-minimizing algorithms and the Hopfield model. The following sections list the questions asked followed by a brief outline of the models proposed to solve them.

## 2. Learning

The main issue taken up in learning is the convergence of local learning rule for feedforward networks. We ask the following question.

### *Learning*

Are there universal (*i.e.*, capable of representing all reasonable functions) feedforward architectures in which the convergence of local learning rule can be proved? By 'local learning rule' we mean those rules which (i) do not use information regarding units to which they are not directly connected, and (ii) do not have large memory requirement.

We propose a network architecture based on finite Fourier series to answer the above question in the affirmative. In this process, we extend the notion of learning to that of learning *functions* from the usual hetero-associative learning. We also propose an attractor model for content addressable memory (a recurrent network) in which learning takes place in the feedforward configuration. Convergence of the learning process is proved in all the models. We also do some peripheral studies relating to tensor product networks, sequence generation, different learning rules, etc.

## 3. Representation

We next take up some representation problems in connectionist modeling. The specific problems taken up are:

### *Validation*

Consider the Hopfield model of content addressable memory. This is an attractor model in which the network dynamics converges to an attractor on every input. The validation problem involves the following two aspects.

1. finding out, in a distributed fashion, whether an attractor corresponds to one of the stored patterns or not;
2. reducing the number of spurious attractors.

### *Multiple objects representation*

Most networks can represent only one object at a time. To represent multiple objects, the networks are usually replicated. This results in the replication of learned information (*i.e.*, connection strengths) in addition to using a large number of units. We explore the following issues: (1) Are there ways of representing multiple objects, without incurring undue overhead in the number/complexity of units? (2) What type of tasks can be performed by such networks?

We call these two representation problems since we expect their solution to be a part of the intrinsic capability of the network structure rather than network operation, *i.e.*, dynamics. This happens to be the case since these two can be solved in *activation*. The solution for both the problems is based on the notion of complex activations.

To solve the validation problem, we introduce complex numbers to the basic model—in this work, the Hopfield network. In the complex domain, the attractors can be both real (binary) and complex. We define genuine attractors as only the real attractors. Now the spurious memories correspond to real attractors which are not one of

the stored patterns. In such models, an input which flows into a complex attractor can be considered novel. This solves one aspect of the problem mentioned above. We have to show that the number of spurious memories is small to solve the second aspect. We propose two ways of complexifying the Hopfield model—the camouflage and the imaginary noise models—and show that the second aspect is also satisfied.

In the camouflage model, we introduce an output function for the units. This function is complex even for binary arguments. The learning rule, which involves the output function, results in complex connection strengths even when binary patterns are stored. In the imaginary noise model, the imaginary part to the connection strengths is noise. In this way, complex numbers can be introduced to the basic model.

For both the models, we calculate the number of binary equilibrium points which we take to be roughly equal to the number of spurious memories. The performance of the camouflage model for small values of  $N$  (the dimensionality of the network) is qualitatively different from that for large  $N$  due to certain approximations that can be done for small  $N$ . We show that for the camouflage model (for small  $N$ ) and for the imaginary noise model

1. the number of spurious memories can be written in the form  $kc^N$ . For certain values of the parameters of the models, we have  $c < 1$ . Thus, for these parameter values, the model is satisfactory.
2. the capacity, the number of patterns that can be made equilibrium points using the *learning rule*, is also satisfactory, though less than that of the Hopfield model.

As mentioned earlier, the multiple objects representation problem is also solved using complex activations. To store  $n$  objects, we choose  $n$  complex numbers, called *basic phases*, such that their possible sums are different. We assign one phase to each object to be represented. The activation pattern for the combination of objects is the superposition of the individual activation patterns. Since the basic phases are chosen such that the possible sums are different, different combination of objects results in different activation patterns.

It is difficult to choose the basic phases satisfying the above requirement. Hence we restrict the scope of representation to those objects in which a feature is present in not more than two objects. This is called the *duo* mode of representation. We give examples of basic phases which can represent up to 5 duo patterns simultaneously. Though the number appears to be small, we indicate how sentences can be represented using this scheme.

We take up an application of the representation scheme proposed—multiple content addressable memories (MCAMs). In MCAMs, more than one pattern can be retrieved in the content addressable mode. Thus the knowledge in the network is used to solve multiple problems without being replicated. We use an existing attractor CAM for storing sparse binary patterns as the basic network. We indicate how three duo patterns can be retrieved simultaneously. We also prove the global stability of two complex Hopfield-like models. (Complex Hopfield-like models have conjugate-symmetric connection matrices.) The MCAM model proposed belongs to one class of such models. We also present some probabilistic calculations on the performance of the network and verify them through simulations.

#### 4. Conclusion

A unifying thread in the models discussed above is the notion of complex activations and weights in neural networks. The use of complex numbers brings a new dimension (both literally and metaphorically) to the neural network dynamics. We have indicated how this can be used in certain cases.

#### References

1. RUMELHART, D. E. AND McCLELLAND, J. L. (EDS) *Parallel distributed processing: Explorations into the microstructure of cognition*, Vol 1, 1986, MIT Press.
2. HOPFIELD, J. J. Neural networks and physical systems with emergent collective computational abilities, *Proc. Natn. Acad. Sci. USA*, 1982, 79, 2554–2558.

### Thesis Abstract (Ph. D.)

## A study of partial discharge characteristics of critical zones in an insulation system of EHV transformer by K. Siddappa Naidu

Research supervisors: R. S. Nema and A. A. Natarajan (NGEF)

Department: High Voltage Engineering

### 1. Introduction

Paper, oil and pressboard are employed in EHV/UHV transformer for insulation system. Partial discharge behaviour has long been identified as an indication for the quality index and the life of transformers. This has assumed greater importance in EHV/UHV range due to the necessity of employing high stresses for optimal design. More scientific approach and data are still called for analysis in the above areas to interpret the partial discharge performance of highly stressed transformer insulation. This will finally lead to the decision of optimal electric stress levels that can be adopted in practice.

Detailed literature survey has revealed that there are many technology gaps in the study of partial discharges and understanding the deterioration of insulation in transformers. These gaps have been identified in an EPL (electrical stress–partial discharge–life) diagram (Fig. 1). There are two approaches to obtain the correlation between electrical stress and the life of insulation system in an EHV transformer: (i) through E–P–L path, and (ii) through E–L path.

Literature survey revealed that a good amount of work has been done in bridging the E–P path, whereas not much work has been done in bridging the P–L path<sup>1–4</sup>. Present technology trend is to follow the E–L path and avoid partial discharges totally in the case of EHV/UHV transformers although the design based on this approach is costly.

### 2. Aim of the work

Efforts have been made in this work to bridge certain gaps by analysing the electrostatic field of the full-scale EHV transformer as well as reduced scale models of critical zones and later conducting experiments on these models. PD inception, extinction, discharge magnitude, pulse distribution, hysteresis characteristics have been studied and presented.

EHV transformer insulation scheme has been conceptualised as having five critical zones based on electrostatic field analysis. They are:

1. Turn-to-turn insulation system ( $\alpha$ ) model,
2. Disc-to-disc insulation system ( $\beta$ ) model,
3. Inter-winding insulation system ( $\gamma$ ) model,
4. Condenser ring region insulation system ( $\delta$ ) model, and
5. High-voltage lead insulation system ( $\eta$ ) model.

### 3. Experimental

A straight detection circuit with a sensitivity of 1 pC with 800 pF sample capacitance has been used for the measurement of partial discharges. Six observations for inception voltage ( $V_i$ ) and extinction voltage ( $V_e$ ) are made and their average is taken. PD magnitude, total number of pulses at different magnitude levels have been measured at inception voltage, at 1.1, 1.2, 1.3  $V_i$  and then at the same voltage levels while reducing up to extinction voltage  $V_e$ .

Extensive experimental work has been done on disc-to-disc insulation system (Fig. 2). The parameters studied are: (1) oil gap 4.5, 5.25 and 6.8 mm, (2) moisture content 8, 17, 24 and 28 ppm, and (3) pressure 30 to 680 torr in steps of 100 torr.

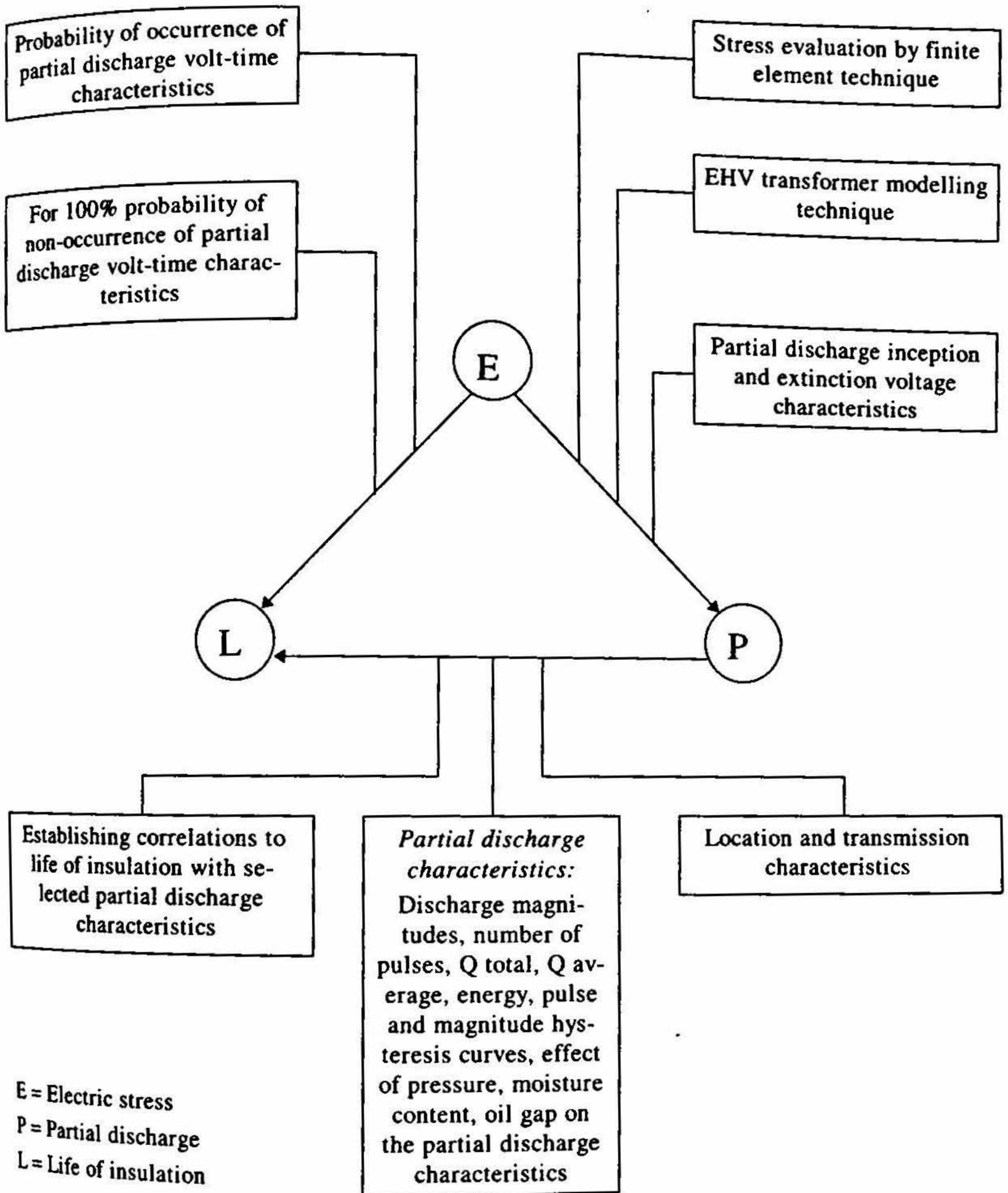


FIG. 1. EPL diagram.

#### 4. Results and discussion

The inception and extinction voltages are found to be decreasing with increase in moisture content of the oil. The pulse distributions have also been studied with increase in moisture content and it is found that the total number of pulses increase with increase of moisture content. The variation of cumulative number of pulses with moisture content at different overvoltages is presented in Fig. 3. The pulse hysteresis curves and magnitude hysteresis plots have also been made and presented. The total discharge magnitude, average discharge magnitude per pulse and

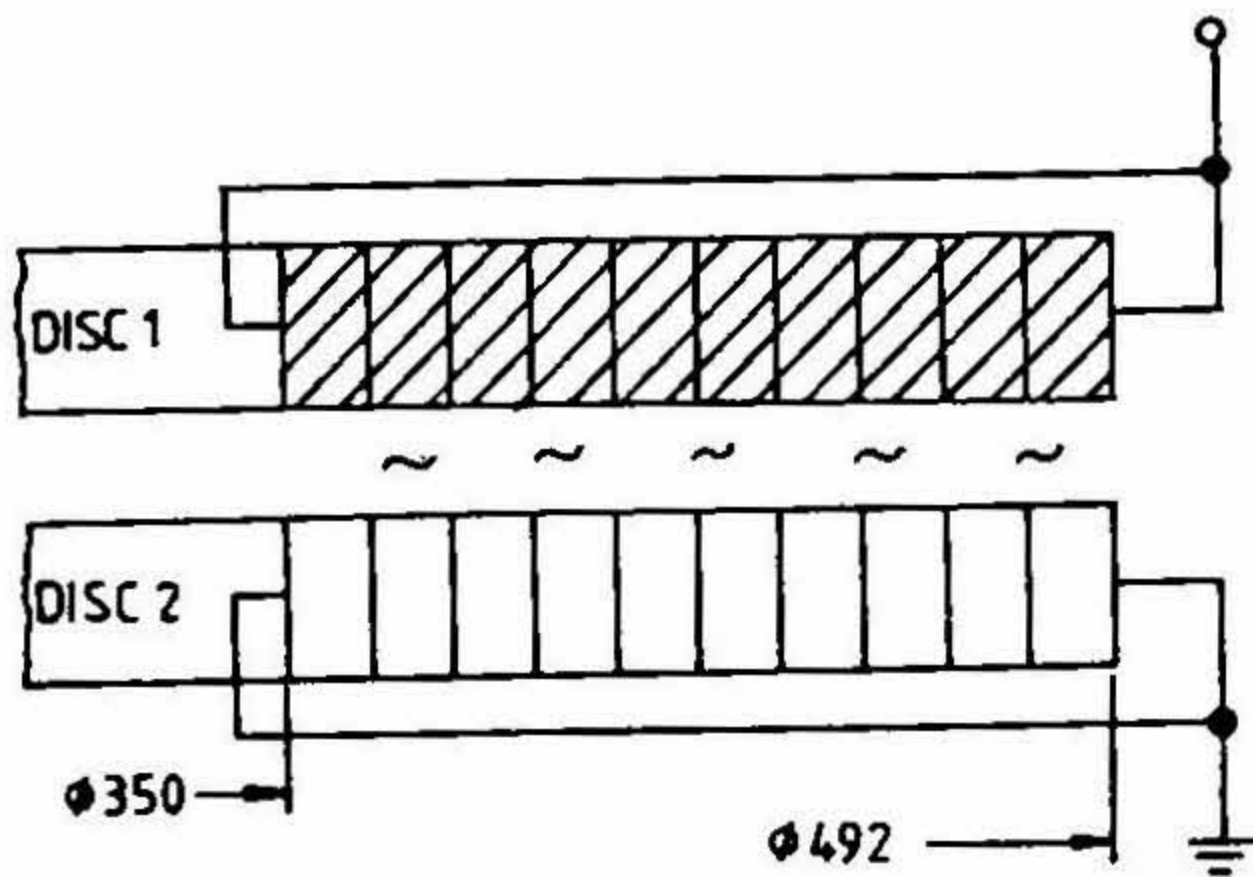


FIG. 2. Schematic diagram of disc-to-disc model.

energy dissipated per cycle have been computed using computer program developed. The variation of these quantities with moisture content has been obtained. The results indicate that the average discharge magnitude per pulse and energy per cycle increase only slightly with moisture content whereas the total discharge magnitude increases steeply with increase in moisture content.

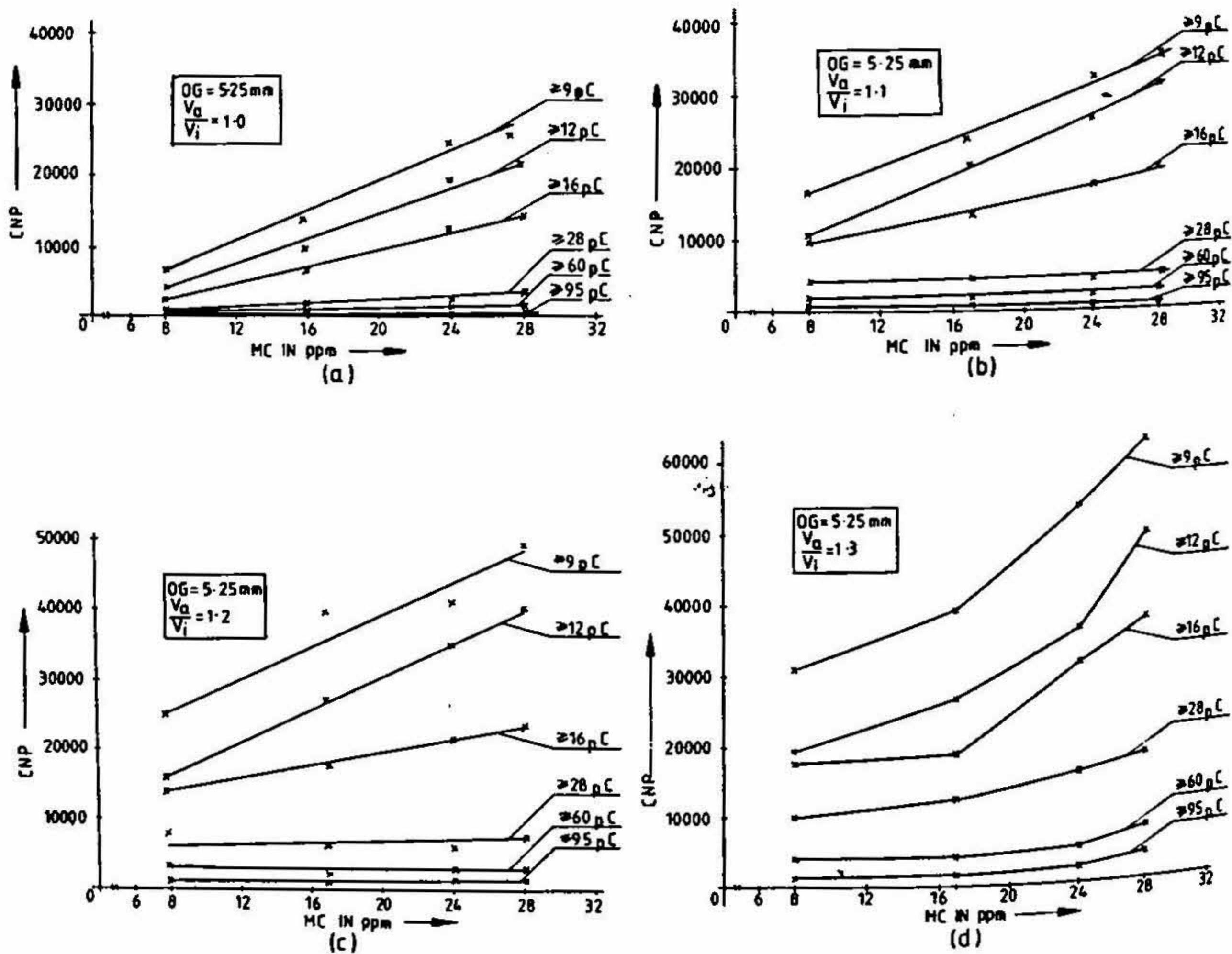


FIG. 3. Variation of cumulative number of pulses with moisture content.

The experiments have been conducted by varying the pressure from 30 to 680 torr inside the chamber. A concept of final extinction voltage has been brought in. The concept of pulse hysteresis curves has been introduced for the first time which has better repeatability than magnitude hysteresis curves.

Considering the complications in predicting the partial discharge performance, another recent approach has been to estimate the threshold stress level of EHV transformer which will not initiate any partial discharge even over the life span of 25 to 30 years. This is achieved by studying the probability of occurrence of partial discharges within a specified duration of electric stress application. This in a way is what is achieved by the EL route in the EPL diagram. Samples of ' $\beta$ ' model have been used to obtain the partial discharge inception voltage-time characteristics. Estimation of the threshold stress level as a sample case has been made. Results obtained from the experiments conducted have been discussed and specifically the estimation has been made of inception voltages using the breakdown criteria. The estimated inception voltages are reasonably in good agreement with experimental values from 680 to 100 torr. Such studies could be extended to all other critical zones to understand the complete insulation system performance of the transformer.

### References

1. YAKOV, S. Volt-time relationship for PD inception in oil paper insulation, *Electra*, December 1979, No. 67, 17-28.
2. IKEDA, M., YANARI, T. AND OKUBO, H. PD and BD probability distribution of equiprobabilistic VT characteristics of oil filled transformer insulation, *IEEE Trans.*, 1982, PAS-101, 2728-2737.
3. YANARI, T. *et al.* Problems of long-term reliability for UHV transformer insulation, *IEEE Trans.*, 1983, PAS-102, 1693-1705.
4. SIDDAPPA NAIDU, K., AGARKHED, S. K., SATYANARAYANA, D. AND NATARAJAN, A. A. Analogue modelling concepts of EHV transformer insulation system, *5th National Power Systems Conf.* 8-10th September 1988, Central Power Research Institute, Bangalore, pp. 302-307.

### Thesis Abstract (Ph. D.)

**Estimation of aircraft aerodynamic derivatives accounting for measurement and process noise by EKF through adaptive filter tuning** by Moses Osmond Gemson

Research supervisors: M. R. Ananthasayanam and K. V. Sreevatsan

Department: Aerospace Engineering

#### 1. Introduction

The most general problem which one encounters in Kalman filtering applications is to deal with nonlinear dynamical equations with unknown parameters as also the statistics of the process and measurement noise and initial state. The filter tuning parameters are the initial state error covariance ( $P_0$ ), the process noise covariance ( $Q$ ) and measurement noise covariance ( $R$ ) which are usually not known a priori to the desired accuracy. Under these circumstances the initial enthusiasm in Kalman filter applications was tempered by the difficulties in properly tuning these filter parameters for divergence-free and near-optimal operation to yield acceptable results. The filter-tuning aspect is a full-fledged nonlinear optimization problem with very few rigorous approaches and generally a manual optimization approach is more prevalent with associated shortcomings. The present work provides a simple heuristic algorithm which utilizes just the quantities which are the output of the Kalman filter to tune it and thus does not demand too much of additional computational load.

#### 2. Adaptive estimation algorithm

A fairly general description of a nonlinear dynamical system in state space representation using a continuous-discrete form is

$$\dot{X}(t) = f(X(t), u(t), \Theta, t) + w(t); E\{X(0)\} = X_0$$

$$z(k) = h(x(k), u(k), \Theta, t_k) + v(k); k = 1, 2, 3, \dots, N \quad (1)$$

where  $X(t)$  is the state variable vector,  $u(t)$ , the control input vector,  $\Theta$ , the unknown parameter vector,  $w$ , the state or process noise vector,  $v$ , the measurement noise vector,  $z$ , the measurement vector,  $t$ , a time instant,  $N$ , the number of measurement points, and an associated cost function required for estimation purposes is

$$J = K_1 \frac{1}{2} (X_0 - X_t)^T P_0^{-1} (X_0 - X_t) + K_2 \frac{1}{2} \sum_{k=1}^N [z(k) - h(\cdot)]^T R^{-1} [z(k) - h(\cdot)] + K_3 \frac{1}{2} \sum_{k=1}^N w(k)^T Q^{-1} w(k) \quad (2)$$

where  $X_t$  is true value of the initial state vector,  $P_0$ , the initial state error covariance matrix which is given by  $E\{(X_0 - X_t)(X_0 - X_t)^T\}$ ,  $h(\cdot)$ , the state-measurement transfer relation,  $R$ , the measurement noise covariance matrix,  $Q$ , the process noise covariance matrix,  $k$ , the sampling index,  $E$ , the expectation operator, and  $K_1$ ,  $K_2$  and  $K_3$  assume values of 0 or 1 depending upon the situation under study. Thus the cost function provides for

- (i) accounting for initial estimates about the states (a priori knowledge),
- (ii) balancing the measurement equations, and
- (iii) balancing the system equations.

The process and the measurement noise are generally assumed to be white Gaussian distributed with zero mean and with nonnegative and positive definite covariances  $Q$  and  $R$ , respectively. Also, the initial state uncertainty is specified as  $P_0$ .

In the extended Kalman filter (EKF) approach the unknown parameters ( $\Theta$ ) are treated as additional states, and the augmented state vector is defined as

$$X_a^T(t) = \{X(t) = \{X(t) | \Theta\}^T \quad (3)$$

in terms of which (1) can be expressed as

$$\dot{X}_a(t) = f(X_a(t), u(t), t) + w(t); X_a(0) = X_{0a}$$

$$z(k) = h(X_a(k), u(k), t) + v(k); k = 1, 2, N. \quad (4)$$

For the above system the Kalman filter algorithm is applied to estimate the augmented states by linearizing the nonlinear equations at the current state estimates. Further, it is known that the filter diverges or gives unacceptable results if  $P_0$ ,  $Q$  and  $R$  are not chosen properly. However, the adaptive estimations of  $Q$  and  $R$  through Myers and Tapley algorithm<sup>1</sup> and  $P_0$  through the Fisher's information matrix<sup>2</sup> with on 'scouting' pass and utilizing them simultaneously in the next pass appears just about the simplest and very effective for parameter estimation applications.

It has been demonstrated subsequently through simulation studies as well as through actual flight test data analysis that a proper combination of  $P_0$  and  $Q$  along with  $R$  provides a near-optimal filter performance.

### 3. Applications

The effectiveness of the above algorithm was demonstrated by analyzing first simulated data which provided a controlled environment. The above simulated experiments mimicked control inputs normally used for aircraft

parameter estimation such as '3211', for example, and the aircraft coefficients (linear and nonlinear ones) used pertain to standard aircraft reported in literature<sup>3,4</sup>. The MMLE algorithm was also further used for validating the EKF algorithm.

Subsequently, a series of flight test data provided in NASA TN D 7831<sup>5</sup> and NASA TP 1690<sup>6</sup> were analyzed using the EKF algorithm. The flight test data analyzed encompass a variety of modelling aspects such as linear and nonlinear representations, dimensional and nondimensional forms of stability derivatives and equations, though uncoupled, still retaining the cross-coupling terms. Some of the salient conclusions arrived at are that the complex optimization requirements manifest as filter-tuning effort and a  $P_0$  and  $Q$  combination would be required along with  $R$  to achieve divergence-free filter performance. The presence of dynamically varying parameters could be tracked by EKF approach, which may not be possible by MMLE because of its batch processing nature.

Even though the present study deals mainly with the application of these techniques to estimate aircraft flight mechanical parameters from flight data, the mathematical algorithms and the computer codes are quite general and can be applied easily to any system governed by a set of dynamical equations as in the present work.

#### References

1. MYERS, K. A. AND TAPLEY, B. D. Adaptive sequential estimation with unknown noise statistics, *IEEE Trans.*, 1976, AC-21, 520-525.
2. SORENSON, H. W. *Parameter estimation principles and problems*, 1980, Marcel Dekker.
3. PLAETSCHKE, E. AND SCHULZ, G. *Practical input signal design*, AGARD-LS-104, paper No. 3, 1979.
4. JATEGAONKAR, R. V. AND PLAETSCHKE, E. Maximum likelihood estimation of parameters in nonlinear flight mechanics systems, *7th IFAC Identification and System Parameter Estimation*, York, UK, 1985.
5. MAINE, R. E. AND ILIFF, K. W. *A FORTRAN program for determining aircraft stability and control derivatives from flight data*, NASA TN D-7831, 1975.
6. MAINE, R. E. *Programmers' manual for MMLE3, a general FORTRAN program for maximum likelihood parameter estimation*, NASA-TP-1690, 1981.

#### Thesis Abstract (Ph. D.)

**A new approach for the numerical solution of constrained mechanical systems by**  
Rachuri Sudarsan

Research supervisors: M. R. Ananthasayanam and S. Sathiya Keerthi

Department: Aerospace Engineering

#### 1. Introduction

The field of kinematics and dynamics of mechanical systems has progressed from a manual graphics art to a highly developed discipline in analytical geometry and dynamics. Various general-purpose formulations for the dynamic analysis of constrained mechanical systems [CMS] lead to mixed differential-algebraic equations [DAEs] called the Euler-Lagrange equations. During the past 15 years many contributions have been made to the theory of computational kinematics and dynamics of CMS (also called multibody dynamics). The recent advances in computer hardware have tremendously revolutionized the analysis of CMS.

While in the past, engineers dealt with small-scale systems that could be analyzed by clever analytical formulations, present-day general-purpose codes permit the design and analysis of complex systems. As the complexity of the systems increases, so does the need for fast and reliable numerical procedures for solving the equations of motion.

This dissertation deals with efficient numerical approaches for solving the Euler-Lagrange equations of motion for CMS. The main objective is to develop a reliable and efficient numerical approach for solving vector

fields and then specialize it to solve the Euler–Lagrange equations of motion for CMS. There are various approaches available for solving the equations of motion for CMS, each having its own strong and weak aspects. Also in the literature these approaches are not studied on a uniform setting. In this thesis, we propose a new approach called ‘Perturbation approach’<sup>1,2</sup> and further provide some improvements to the existing approaches. A careful analysis of the computational cost for each of the approaches is done and a thorough numerical testing is carried out. All the approaches are then compared in common setting. Recommendations are made about the choice of the approach and the numerical integration method to be used in solving problems in CMS.

## 2. Vector fields

We begin by formally defining the vector field that is to be solved numerically. Let  $\mathcal{M}$  be an  $(n-m)$  dimensional manifold in  $R^n$  defined by

$$g(x) = 0, \quad (1)$$

where  $g: R^n \rightarrow R^m$  is a smooth function. Assume that  $\exists$  is an open set  $\mathcal{O}$  in  $R^n$  containing  $\mathcal{M}$  such that  $g_x(x)$ , the  $m \times n$  Jacobian of  $g$  at  $x$ , satisfies  $\text{Rank}(g_x(x)) = m \forall x \in \mathcal{O}$ . Let

$$\dot{x} = \frac{\Delta dx}{dt} = f(x), \quad t \in [t_0, t_f], \quad (2)$$

define a vector field on  $\mathcal{M}$ . In other words, if  $T_x\mathcal{M}$  denotes the tangent space of  $\mathcal{M}$  at  $x \in \mathcal{M}$ , then  $f(x) \in T_x\mathcal{M} \forall x \in \mathcal{M}$ . Usually a smooth extension of  $f$  to an open set in  $R^n$  containing  $\mathcal{M}$  is available. We will assume this to be the case for, when dealing with numerical methods points slightly off from  $\mathcal{M}$  are obtained and there may be a need to evaluate  $f$  there.

As already mentioned, the main objective is to develop a reliable and efficient numerical approach for solving a vector field of the form (2) defined on the manifold  $\mathcal{M} = \{x: g(x) = 0\}$  and then specialize it to solve the Euler–Lagrange equations of motion for CMS. The problem of numerically solving (1)–(2) arises in a number of applications, such as simulation of control systems modeled by DAEs, numerical curve tracing, homotopy curve tracing, handling physical invariants, and constrained optimization.

## 3. Constrained mechanical systems

Since our emphasis is on the solution of the equations of motion for CMS, let us briefly define the Euler–Lagrange equations. To solve the Euler–Lagrange equations of motion for CMS, we derive the special vector field associated with it and specialize the numerical approach developed for solving the general vector fields.

The Euler–Lagrange equation that describes the motion of CMS can be written in the form<sup>3</sup>

$$M(q)\ddot{q} + J^T(q)\lambda = Q(\dot{q}, q) \quad (3)$$

$$0 = \phi(q), \quad (4)$$

where  $q \in R^n$  is the vector of generalized coordinates,  $M(q) \in R^{n \times n}$  is the generalized mass matrix,  $\phi: R^n \rightarrow R^m$  is a nonlinear mapping that defines the constraints (kinematical),  $J = \partial\phi/\partial q$  is the Jacobian of  $\phi$  with respect to  $q$  ( $J^T$  denotes the transpose  $J$ ),  $\lambda \in R^m$  is the vector of Lagrange multipliers associated with the constraints, and  $Q: R^n \times R^n \rightarrow R^n$  is a mapping that defines generalized external forces. Here time invariance of  $M$ ,  $\phi$ ,  $Q$ , and  $J$  is assumed only to simplify the notations. The system of eqns (3) and (4) is an index-3 DAE. The index can be lowered by a procedure called index reduction. The index-1 form of the Euler–Lagrange equations can be written as,

$$\begin{bmatrix} M(q) & J^T \\ J & 0 \end{bmatrix} \begin{bmatrix} \ddot{q} \\ \lambda \end{bmatrix} = \begin{bmatrix} Q(\dot{q}, q) \\ v(\dot{q}, q) \end{bmatrix} \quad (5)$$

$$\phi(q) = 0 \quad (6)$$

$$\dot{\phi} = J\dot{q} = 0. \quad (7)$$

Under reasonable assumptions on  $M$  and  $J$ , the linear system in  $\dot{q}$  and  $\lambda$  defined by (5) has a unique solution

$$\begin{aligned} \ddot{q} &= f_1(\dot{q}, q); \\ \lambda &= f_2(\dot{q}, q). \end{aligned}$$

If we let  $\dot{q} = v$ ,  $x = (q, v)'$  then we have

$$\begin{aligned} \dot{q} &= v \\ \dot{v} &= f_1(\dot{q}, q), \end{aligned} \quad (8)$$

together with

$$\phi(q) = 0; Jv = 0. \quad (9)$$

Equations (8) and (9) can be written in the form

$$\dot{x} = f(x) \quad (10)$$

$$g(x) = 0, \quad (11)$$

respectively. Equation (10) defines a vector field on the constraint manifold defined by (11) and it has some special structure which can be exploited while implementing.

Each  $f$  evaluation involves the solution of the linear system (5), whose coefficient matrix has a nice  $(2 \times 2)$  block structure. In most examples in CMS, the matrices  $M(q)$  and  $J(q)$  are sparse. Special techniques like block factorization and sparse matrix algorithms should be employed. For large systems, it is advantageous and preferable to use iterative methods, *i.e.*, solving the linear system as an optimization problem. Also note that eqn (7) is linear in  $v$ .

#### 4. Existing numerical approaches

Let us assume that the vector field, (2), is solvable, *i.e.*, given any  $x_0 \in \mathcal{M}$  there exists a unique solution,  $x: [t_0, t_f] \rightarrow \mathcal{M}$  that satisfies  $x(t_0) = x_0$  and (2). Our aim is to obtain a numerical approximation of  $x(\cdot)$ . Since the facts,  $x_0 \in \mathcal{M}$  and  $x(\cdot)$  satisfies (2), automatically guarantee  $g(x(t)) = 0 \forall t \in [t_0, t_f]$ ; we can simply ignore (1) and numerically solve (2) using any well-known integration method for ordinary differential equations (ODEs) to obtain an approximate solution,  $\tilde{x}(\cdot)$ . There are two strong objections to such an approach which excludes (1) from the solution process: (i)  $\tilde{x}$  may violate (1) badly; and (ii) the information that (1) is an invariant along the solution can be used to check, and perhaps improve, the accuracy of the solution.

Methods which try controlling the global error are very expensive. All popular integration codes only employ local error control where integration is done *via* a number of successive time steps, the computations in one time step being done as if integration in the previous time steps was done exactly. When local error control is used, the violation of (1) can build up and become huge for large  $t$ . Since (1) is a fundamental constraint in our problem, a huge violation of it is certainly objectionable. In this thesis we give an example illustrating a case of severe violation in (1).

There are various approaches available for solving CMS. These are: (i) Parametrization, (ii) Inexact constraint stabilization [ICS], and (iii) Exact constraint stabilization [ECS].

The parametrization approach establishes a minimal set of ODEs using a coordinate transformation (this transformation is obtained numerically) which is then solved using standard ODE techniques. The solution of CMS in the original coordinate system is then obtained using the inverse of the above transformation. That is,  $\mathcal{M}$  is locally parametrized around a given initial point,  $x_0 \in \mathcal{M}$ :

$$x = \psi(y), \quad (12)$$

where  $\psi: \Theta_y \rightarrow \Theta_x \cap \mathcal{M}$ ,  $x_0 = \psi(0)$ ,  $\Theta_y$  is an open set in  $R^{n-m}$  containing the origin,  $\Theta_x$ , an open set in  $R^n$  containing  $x_0$ , and  $\psi$ , a diffeomorphism. This parametrization is used to replace (2) by a differential equation in  $y$ :

$$\dot{y} = \tilde{f}(y). \quad (13)$$

The determination of  $\psi(y)$  and  $\tilde{f}(y)$  given  $y$  is simultaneous and requires the numerical solution of a square system of  $m$  nonlinear equations. The parametrization approach consists of solving (13). The coordinate partitioning approach<sup>3</sup> and tangential parametrization (TP) approach<sup>4</sup> are specific instances of this approach. The coordinate partitioning approach was initiated by Wehage and Haug<sup>5</sup> and has been popularly used for solving CMS. As the name suggests, the generalized coordinate vector is partitioned into independent and dependent set of vectors. It is theoretically possible to locally reduce a vector field to a minimal set of ODEs in terms of independent coordinates. This ODE can be numerically integrated using any well-known method. The idea of TP was introduced by Mani *et al.*<sup>4</sup> and its framework is based on putting an orthogonal coordinate system on the tangent space of the manifold.

In the ICS approach<sup>5</sup>, as applied to CMS, the second time derivative of  $\phi$  is replaced by

$$[J(q)\ddot{q} - v(q, \dot{q})] + \alpha [J(q)\dot{q}] + \beta [\phi(q)] = 0, \quad (14)$$

*i.e.*,  $\ddot{\phi} = 0$  is replaced by the equation  $\ddot{\phi} + \alpha \dot{\phi} + \beta \phi = 0$ , which makes  $\phi = 0$  stable if  $\alpha$  and  $\beta$  are chosen to be positive. Then the ODE system, derived by solving (4) and (5) for  $\ddot{q}$  (and  $\lambda$ ), is simply solved to obtain a solution of the dynamical system. The advantages of the approach are that it is simple and efficient. However, it suffers from important defects such as: (i) a lack of a systematic way to choose  $\alpha$  and  $\beta$ , (ii) the effect of  $\alpha$  and  $\beta$  on the accuracy of the numerical solution, and (iii) the effect of  $\alpha$  and  $\beta$  on the stiffness of the ODE.

In the ECS approach<sup>6</sup>, as applied to (2) and (1), (2) is replaced by

$$\dot{x} = f(x) - g_x^T(x)\mu, \quad (15)$$

so that (15) and (1) form a system of differential-algebraic equations (DAEs) in  $(x, \mu)$ . It can be easily shown that  $\mu = 0$  along every solution of (15) and (1). Thus, this DAE system is the same as the vector field, (2)–(1) and its numerical solution using an appropriate DAE method (*e.g.*, using backward difference formulas) yields a solution of (2) and (1). The approach can be nicely specialized to CMS<sup>6</sup>. The advantage of this formulation is that the position and velocity level constraints are automatically satisfied. The extra variables are not really much of a disadvantage because the computations can be arranged in a form that avoids the storage of the new variables. A computationally efficient modification of this approach is discussed in this thesis. The cost per integration step of this approach is only slightly more than that of the perturbation approach. However, it is easy to see that the exact constraint stabilization approach will require many more integration steps to complete a solution since it can employ only the restricted set of DAE methods.

## 5. Contribution of the thesis

In this thesis, we propose a new approach called 'Perturbation approach' [PA] and also improve the existing approaches so as to have a unified theory of all the existing approaches and the new approach. A careful computation cost analysis of each of the approaches is done and a thorough numerical testing is carried out. All the approaches are then compared in common setting. Recommendations are made about the choice of the approach and the numerical integration method to be used.

The main idea of the perturbation approach is the following. The ODE defining the vector field on the constraint manifold is numerically integrated and after each integration step the numerical solution is perturbed in some suitable way so as to find a point on the manifold and thus get a more accurate solution than before.

To describe the approach it is sufficient to say what is done in one integration step. Suppose  $k$  steps of the numerical solution of (1)–(2) have been done using the approach and  $t = t_k$  has been reached. Let  $x_k \in \mathcal{M}$  be the solution approximant at  $t = t_k$ . Denote the local solution by  $x(\cdot)$ , *i.e.*,  $x(\cdot)$  is the solution of (2) with  $x(t_k) = x_k$ . Let  $\tau$  denote the integration tolerance. In the  $(k + 1)$ st step ( $t_{k+1} = t_k + h_k$ ), the aim is to determine a step size  $h_k$  and an  $x_{k+1} \in \mathcal{M}$  that satisfy

$$\|x(t_{k+1}) - x_{k+1}\| \leq \tau. \quad (16)$$

The determination of  $h_k$  and  $x_{k+1}$  is described by the following procedure.

*Procedure PA:* Determination of  $h_k$  and  $x_{k+1}$  by the perturbation approach.

1. Numerically integrate (2) from  $x(t_k) = \bar{x}_k$  using local error control (without concerning (1)) to obtain a step size  $h_k$  and an approximant,  $\bar{x}_{k+1}$  that satisfy

$$\|x(t_{k+1}) - \bar{x}_{k+1}\| \leq \tau/2. \quad (17)$$

2. Solve the optimization problem

$$\min \|x - \bar{x}_{k+1}\| \text{ s.t. } g(x) = 0; \quad (18)$$

and set  $x_{k+1}$  = the minimizer of (18).

The perturbation approach proposed in this dissertation overcomes some of the difficulties faced with the other existing approaches. The salient features of this approach are: (i) it decouples the process of integration from the process of correction to the constraint manifold, (ii) it solves the vector fields in terms of the original coordinates and hence the integration tolerances for the original variables can be specified directly, and (iii) it does not involve any coordinate transformation which has to be carried out in some of the other approaches and hence there is no necessity for integration restart.

An important issue concerning integration error control has not been carefully addressed in the literature for parametrization approach. In this thesis, we suggest a way for specifying these tolerances which is very important in any good implementation of the approach.

We argue that the perturbation approach is better than the parametrization approach. The chief defects of the parametrization approach are that: (i) each  $\tilde{f}$  evaluation requires the solution of an  $m$ -dimensional nonlinear system of equations apart from one  $f$  evaluation, and (ii) since the parametrization is local, a change in parametrization may be required during the solution, leading to an integration restart with associated inefficiencies. The perturbation approach does not suffer from these defects. It requires only one solution of an  $m$ -dimensional nonlinear system of equations in each integration step (Step 2 of Procedure PA). Also, it does not require any integration restarts because it deals with the full ODE system in (2). The parametrization approach has the advantage that it integrates only the  $(n-m)$ -dimensional system of ODEs, (13), whereas the perturbation approach requires the integration of the  $n$ -dimensional system of ODEs, (2). This advantage, however, is only slight because the difference in the integration overhead costs of the two approaches is only  $O(m)$  whereas the cost of every extra  $m$ -dimensional nonlinear system solution required by the parametrization approach is  $O(m^3)$ .

The four approaches (PA, TP, ECS, ICS) have been carefully coded and compared on some test problems. The perturbation approach has a number of advantages over existing approaches. The testing quantifies and confirms the qualitative comparisons mentioned above.

#### References

1. KEERTHI, S. S., SUDARSAN, R. AND SANCHETI, N. K. A new approach to the numerical solution of constrained mechanical system dynamics, *Proc. IEEE Int. Conf. on Robotics and Automation*, Nice, France, 1992.
2. SUDARSAN, R. AND KEERTHI, S. S. Comparison of numerical approaches to the simulation of constrained mechanical system dynamics, *Proc. Summer Computer Simulation Conf., SCSC 92*, Nevada, 1992.
3. HAUG, E. J. *Computer aided kinematics and dynamics of mechanical systems*, Vol. I: Basic methods, 1989, Allyn and Bacon.
4. MANI, N. K., HAUG, E. J. AND ATKINSON, K. E. Application of singular value decomposition for analysis of mechanical system dynamics, *Trans. ASME, J. Mech. Trans., Aut. Des.*, 1985, 105, 82-87.

5. WEHAGE, R. A. AND HAUG, E. J. Generalized coordinate partitioning for dimension reduction in analysis of constrained dynamic systems, *Trans. ASME, J. Mech. Des.*, 1982, 104, 247-255.
6. BAUMGARTE, J. Stabilization of constraints and integrals of motion in dynamical systems, *Comput. Meth. Appl. Mech. Engng*, 1972, 1, 1-16.
7. GEAR, C. W., LEIMKUHNER, B. AND GUPTA, G. K. Automatic integration of Euler-Lagrange equations with constraints, *J. Comput. Appl. Math.*, 1985, 12, 77-90.

### Thesis Abstract (Ph. D.)

## Transonic flow of a real fluid and some problems using a new theory of shock dynamics by D. Chandrasekar

Research supervisor: Phoolan Prasad

Department: Mathematics

### 1. Introduction

This thesis embodies the results of investigation of two important problems in gasdynamics: (i) the transonic flow of a real fluid through a nozzle of varying cross-section and (ii) the propagation of a shock wave of arbitrary strength in a polytropic gas. The thesis starts with a discussion of the relevant literature on shock waves and the controversies over the transonic flows, and a discussion of the importance of the fundamental derivative

$\bar{\Gamma} = \frac{1}{\rho} \frac{\partial(\rho a)}{\partial p} \Big|_s$ , ( $\rho$ , the density,  $a$ , the velocity of sound and  $s$ , the entropy of the fluid) in gasdynamics, in the con-

text of nonlinear wave propagation is also discussed. The qualitative difference in the behaviour of nonlinear wave having both positive and negative nonlinearity in the same pulse, from that of nonlinear wave with either positive or negative nonlinearity has been explained<sup>1</sup>. A brief account of the important influence of the nonlinear waves that catch up with the shock from behind has been included to explain the importance of these waves in finding the successive positions of a shock wave.

### 2. Steady transonic flow of a real fluid

An approximate equation governing the steady transonic flows near the throat of the nozzle has been derived, based on the assumption that the fundamental derivative changes its sign in a small neighborhood containing the throat of the nozzle. A phase-plane analysis of the model equation shows that unlike in the case of an ordinary gas, there are two sonic points at which the flow changes from subsonic to supersonic or *vice versa*. The nature of the singular point (either a saddle or centre) is found to depend on the sign of the product of the curvature  $k$  of the nozzle at the throat and the value of  $\bar{\Gamma}$  at the sonic point ( $\hat{\Gamma}$ ). Continuous steady flows are found to be possible only through one of the sonic points at which  $k\hat{\Gamma}$  is positive. Compression and expansion shock waves have been shown to exist in a transonic flow. Further, steady sonic shock waves (*i.e.*, shock waves having either the up or the downstream sonic velocity) are not only possible but necessary in some transonic flows. Various possible steady flows near the throat of the nozzle are discussed in the phase-plane.

### 3. Propagation of nonlinear waves on steady transonic flows in a nozzle

A transonic wave, whose amplitude  $\epsilon$  is small and of the order of the fundamental derivative at the sonic point, moving upstream of the flow in a nozzle, is modelled by a single first-order partial differential equation. This equation belongs to a class of conservation laws with a non-convex flux function having an inhomogeneous source term. These waves are found to stay in the transport region, for time intervals of order  $\epsilon^{-1/2}$  and extend over the throat region of order  $\epsilon^{3/2}$ . The numerical evolution of these waves on the steady transonic flows is carried out to study the logical stability of the steady flows. A brief account of the 'singularity separating method' and its modified version incorporating the source term has been included. This method has been used to numerically integrate the model equation. The local stability of various steady transonic flows near the throat has been studied in detail.

#### 4. Propagation of a plane shock wave

The difficulties encountered in finding the successive positions of a shock wave both by analytical and numerical methods are reviewed. A brief account of the new theory of shock dynamics of Ravindran and Prasad<sup>2</sup> for the determination of the successive positions of a shock of arbitrary strength is given for the simple model equation  $u_t + uu_x = 0$ . The system of compatibility conditions on the shock path<sup>3,4</sup> takes into account the influence of the nonlinear waves that catch up the shock from behind. This theory gives the accurate position and strength of the shock. The first three compatibility conditions on the shock path are derived for a shock of arbitrary strength.

The successive positions of a shock of arbitrary strength arising out of the motion of an accelerating piston moving with a nonzero velocity into a polytropic gas at rest have been calculated. The system of compatibility conditions is integrated numerically to give the evolution of the shock position and strength at various times. A comparison between the solution obtained by Lax-Wendroff method and the new theory of shock dynamics has been made to demonstrate the various advantages of the new theory over the finite difference method. The solution of the compatibility conditions not only gives the accurate position and the strength of the shock but also the entire solution behind the shock in less computational time compared to the finite difference scheme.

#### References

1. CRAMER, M. S. AND KLUWICK, A. On the propagation of waves exhibiting both positive and negative nonlinearity, *J. Fluid Mech.*, 1984, 142, 9-37.
2. RAVINDRAN, R. AND PRASAD, P. A new theory of shock dynamics: Part I, *Appl. Math. Lett.*, 1990, 3, 77-81.
3. GRINFEL'D, M. A. Ray method of calculating the wave front intensity in nonlinear elastic material, *PMM J. Appl. Math. Mech.*, 1978, 22, 787-793.
4. MASLOV, V. P. Propagation of shock waves in an isentropic non-viscous gas, *J. Sov. Math.*, 1980, 13, 119-163.

#### Thesis Abstract (M.Sc.(Engng))

### Optimum design of composite laminates for buckling, vibration and interlaminar strength by ranking by M. Kumar

Research supervisors: K. P. Rao, A. V. Krishna Murthy and K. Vijayakumar

Department: Aerospace Engineering

#### 1. Introduction

Fibre reinforced plastics [FRP] are extensively used in many aerospace structures due to their superior material properties and the possibility to tailor them for each specific application. The design of such a material system involves several parameters such as choice of resins, fibres, ply thicknesses and fibre orientations. Often prepregs are used to build laminates and the thickness of a prepreg ply is so small that it is necessary to use many plies to build the required thickness of the laminate. In view of a large number of design variables involved, proper choice of parameters such as fibre orientations requires special design procedures. The present work enables one to arrive at the optimum fibre orientations for specific design problems.

In the present study, it is assumed that the laminate is made of repeated sublaminates<sup>1</sup> with each sublaminate consisting of a smaller number of plies, for example, 2 to 8; we consider quadri-, tri- and bidirectional laminates. This leads to a more damage-tolerant design. Considering all possible stacking sequences, a set of 1128 sublaminates schemes are considered (840 cases of 8 ply, 240 cases of 6 ply, 36 cases of 4 ply and 12 case of 2 ply). The fibre orientation chosen in each ply of the sublaminate is such that the laminate gives an optimum structural performance. This can be accomplished very conveniently using ranking technique in which a structural performance parameter of the laminate is evaluated for each possible configuration of the sublaminate and com-

pared to arrive at the best lay-up. This procedure can be very conveniently implemented on computers. Simple computer programs for optimum design (for buckling/vibration/interlaminar strength) are developed in this work which can be implemented on modern personal computers.

## **2. Optimum design of composite laminates for buckling**

Buckling is one of the important failure modes of composite laminates. Optimizing the orientations of the plies in each sublaminates is attempted in order to achieve maximum buckling load for the given laminate thickness or minimum thickness for the given buckling load. Using orthotropic plate theory<sup>2</sup> buckling loads are obtained for various loading and boundary conditions. A computer program has been developed wherein the buckling load is calculated for the 1128 sublaminates schemes and rank ordered. The laminate scheme which is at the top of the ranking table is the optimum laminate scheme from the buckling point of view. The program also has been modified to enable the designer to arrive at the required thickness of the laminate with optimized orientations for a given buckling load, boundary conditions and geometry.

## **3. Optimum design of composite laminates for vibration**

Dynamic loads on structures give rise to large dynamic displacements and stresses. Thus it is essential to design a composite laminate for dynamic response in addition to static loading. The dynamic behaviour mainly depends on the natural frequencies of laminate. The natural frequencies of a laminate are influenced by choice of material, lay-up sequence and geometry. Generally, the dynamic response is considered to be better when the fundamental frequency is high or the separation between the fundamental and the second frequency is large. Therefore, the choice of lay-up should be such that the laminate has the highest possible natural frequency (the difference between the fundamental and the second frequency). In the present study, ranking technique is used together with orthotropic plate theory<sup>3</sup> to find the optimum lay-up (a) for maximum fundamental frequency, (b) for maximum difference between the fundamental and the second frequency, (c) for minimum thickness laminate for a given fundamental frequency, and (d) for minimum thickness of laminate for a given difference between the fundamental and the second frequency. Six different boundary conditions are considered. Nine different materials which are commonly used in aerospace engineering are available in the materials library of the computer code developed for this purpose.

## **4. Optimum design of composite laminates for interlaminar strength**

Delamination is one type of defect or damage, which is nothing but ply separation or debond between adjacent layers. Interlaminar failures may cause either embedded delamination or a free edge delamination which in turn will influence the stiffness and strength of the laminate. Delamination may result from discontinuities in the structure, such as ply terminations or ply drop for tapering the thickness and/or free edges under impact, inplane or thermal loading. High interlaminar stresses arise because of mismatch in material mechanical properties and/or the presence of stress gradients as in the case of the free boundaries. Therefore, interlaminar stresses must be considered whenever composite laminates are used in a structure which has free edges or cutouts. Interlaminar stresses in a composite laminate may be controlled to a large extent by the proper choice of materials, fibre orientations, stacking sequence and layer thickness. The criterion for delamination occurrence and the process of its development depends on several parameters. In the present work, a simple criterion<sup>4</sup> is adopted which is well known for the case of a laminated coupon. With the aid of this example a methodology is developed for optimally choosing the lay-up using the ranking technique. The methodology and the software developed are validated by comparing results available in the literature. Using fracture mechanics approach, the delamination in the form of an edge crack is assumed at the interface. The delamination onset occurs when strain energy release rate reaches certain critical values. Strain energy release rate is calculated at each and every interface, one after the other, starting from the laminate extreme interfaces till the midplane of the laminate. Out of the strain energy release rates calculated for all the interfaces of a laminate, the maximum value of strain energy release rate for that particular laminate is stored. Likewise, 840 cases of 8 ply sublaminates, 240 cases of 6 ply sublaminates, 36 cases of 4 ply sublaminates, 12 cases of 2 ply sublaminates are considered depending upon the number of plies present in each sublaminates and the maximum strain energy release rate along with the laminate code is stored. Laminates are rank ordered along with the laminate code in the order of increasing values of the strain energy release rate.

The laminate code which has the least value of strain energy release rate would be at the top of the table and this laminate will be the best from the point of view of resistance to delamination occurrence.

### 5. Conclusions

In this work the possibility of designing composite laminates optimally by using ranking technique for achieving (i) maximum buckling load or (ii) maximum fundamental frequency/maximum difference between the first and the second frequencies or (iii) maximum delamination resistance have been investigated. User-friendly menu-driven computer programs implementable on personal computers have been developed and validated to achieve this objective. A new strategy to obtain the minimum composite laminate thickness required along with the fibre orientations in various plies for a specified (a) buckling load or (b) fundamental frequency or (c) difference between the first and the second frequencies has also been used in the computer code and validated by studying typical cases.

### Reference

1. TSAI, S. W. *Composites design*, 4th edn, Section 24, 1988, Think Composites.
2. LEKHNITSKII, S. G. *Anisotropic plates*, 1968, Gordon and Breach.
3. WHITNEY, J. M. *Structural analysis of laminated anisotropic plates*, p. 122, 1987, Technomic Publishing.
4. SCHANZ, U. AND KRESS, G. Influence of temperature and moisture on total strain energy release rates associated with edge delamination of composite test coupons, *Comput. Sci. Technol.*, 1989, 35, 219-233.

### Thesis Abstract (M. Sc. (Engng))

#### Analysis of buffering for a shared medium fast packet switch by B. K. Jayaram

Research supervisor: Utpal Mukherji

Department: Electrical Communication Engineering

### 1. Introduction

A shared medium fast packet switch<sup>1</sup> consists of a shared medium which performs the basic switching function of transferring packets from inputs to outputs, inputs, which receive packets from the input links, buffer them as necessary, and send them through the shared medium, and outputs which receive packets from the shared medium, buffer them as necessary, and transmit them over the output links.

All buffers are assumed to be composed of first-in-first-out queues. A packet arrives over an input link in a high-speed serial bit stream. The input extracts the packet, performs a serial to parallel transfer, and stores it in its buffer. Once a complete packet is stored, it signals the shared medium that it has a packet to transmit. Only one input can have access to the shared medium at any time. A central controller is responsible for resolving contention for access among the various inputs. For simplicity, it may be assumed that no separate arbitration delay is experienced. Once an input has access to the broadcast shared medium, it transmits one or more complete packets at the speed of the medium, which is typically many times that of the input links. The output for a packet is identified by an address included in the packet header. All outputs receive the packets, but only the output identified by the header address copies the packet into its buffer. The output transmits the packet on the serial output.

Input analysis is concerned with packets from the time they arrive over input links till they are placed in output buffers. Similarly, output analysis is concerned with packets from the time they are buffered at outputs till they are completely transmitted over output links.

In analysis found in literature, assumptions are made that all input links have equal capacity and that the capacity of the shared medium is at least equal to the sum of the capacities of all input links. When the shared me-

dium server uses the round-robin exhaustive service discipline, it is known from numerical methods that the number of bits at any input is upper bounded by  $3.3502 P$  where  $P$  is the maximum packet size in bits<sup>1</sup>. Closed-form expressions can be derived for the upper and lower bounds on the number of bits at any input under the round-robin exhaustive service discipline from which it is known that  $3.051 P \leq \text{number of bits at an input} \leq 3.307 P$  for this discipline<sup>2</sup>. For real-time gated service discipline it is known that the number of bits at any input is upper bounded by  $3.00 P^2$ . A Markov-modulated continuous flow model has been proposed to approximate the packet arrival process to an output queue<sup>3</sup>, in which packet sizes are assumed to be exponentially distributed and destinations are chosen independently for all packets, and from which queue length distributions are obtained for both infinite and finite buffer sizes at the outputs.

This work presents input and output analyses under the assumption that packets have a fixed size. Input analysis is presented for both the equal and unequal input link capacity cases. The case of a slow shared medium server is also considered, where the service capacity is less than the sum of the capacities of all input links.

## 2. Input buffering for equal capacity links

$N$  input links that have equal capacity are considered. The shared medium capacity is assumed to be  $N$  times the capacity of an input link. The queueing theoretic concept of work in the system is used in modelling the buffering problem. A link generates work at a rate of  $1/N$  units per unit time when it is active. Each packet constitutes  $1/N$  units of work. Work is forwarded by the link to the shared medium server in packets at intervals of one time unit when a link is active. After a link forwards a packet to the server, it may continue to generate another packet or become idle again. Once idle, the link remains in that state for an arbitrary duration of time. The links become active independent of one another. The server is assumed to be work conserving, and serves at a rate of 1 unit of work per unit time while unfinished forwarded work is present. Service is non-preemptive in that the server completes service of a packet before beginning the service of another packet.

It is shown that (i) the buffering required for any input link is not more than  $1 + (N-1)/N$  packets, and (ii) the total number of packets stored at a time in the input buffers is not more than  $N$ .

## 3. Input buffering for links with unequal capacities

$N$  input links which may have different capacities are considered. The capacity  $M$  of the shared medium server is assumed to be equal to the sum of the capacities of the input links. Two work-conserving service disciplines are considered for the shared medium. The earliest forwarding time first (FCFS) packet service discipline is known to minimise maximum packet delay<sup>4</sup>. The service discipline that serves the packet from the link with the earliest next packet forwarding due time is known to result in a uniform buffer requirements of 2 packets on all input links in the case when service preemption takes place<sup>5</sup>.

The buffering problem is modelled in terms of the queueing theoretic concept of work in the system, and it is shown that: (i) the total number of packets stored at a time in all the input buffers is not more than  $N$ , (ii) the FCFS service discipline gives a uniform upper bound of  $N/M$  time units on the delay of a packet on an input link, and (iii) the earliest due time based non-preemptive service discipline results in a uniform buffer requirement of 2 packets on all input links.

## 4. Output buffering for links with equal capacity

Each output link is assumed to follow a work-conserving FCFS service discipline. The intervals between successive instants at which packets are forwarded by the shared medium to an output link must be of duration at least equal to the time the shared medium requires to serve a packet. When all  $N$  input and  $N$  output links have equal capacity and the capacity of shared medium is equal to the sum of the capacities of the  $N$  input links, an output link requires 1 time unit to transmit a packet and the packet service time of the shared medium is  $1/N$ . This suggests a discrete time queueing model for output buffering with the discrete time unit taken equal to the packet service time of the shared medium.

An ideal packet-forwarding process is considered. Assume that an input link  $k$  can turn active only at the times  $t = i + (k-1)/N$ ,  $i = 0, 1, 2, \dots$ ,  $k = 1, 2, \dots, N$ . Assume that input links forward packets to the shared me-

dium in independent Bernoulli processes with parameter  $p_l$ , and that the output links for packets are chosen equiprobably among all output links in independent Bernoulli trials. Such a traffic pattern has been termed uniform and independent<sup>6</sup>. In this process, a packet is forwarded to output link  $k$  with probability  $p_l/N$ , independently at each of the times  $t = 1 + (l + 1)/N$ ,  $l = 0, 1, 2, \dots$ . Hence, an output link is a geometric/deterministic/1 queueing system with Bernoulli arrival probability  $p_l/N$  and deterministic service time equal to  $N$  arrival time units, and thus<sup>7</sup> has a mean packet delay  $(2 - \frac{N+1}{N} p_l) / (2(1 - p_l))$ .

It is shown using simulations that geometric/deterministic/1 output queueing models are appropriate for a variety of input link packet forwarding processes.

### 5. The slow shared medium switch

Output queueing behaviour when the capacity of the shared medium is less than the sum of the input link capacities is similar to that discussed in Section 4 where the capacity of the shared medium equalled the sum of the link capacities. The difference between the two cases is due only to the fact that the time required by the output link to transmit a packet is a smaller multiple of the packet service time of the shared medium. For the ideal packet forwarding process of Section 4, the intervals between successive instants at which packets are forwarded to the shared medium are multiples of  $1/N$ . If the packet service time of the shared medium is also a multiple of  $1/N$ , then the input buffering also has similar behaviour.

It is shown using simulations that geometric/deterministic/1 queueing models are appropriate for both input and output buffering.

### References

1. CIDON, I., GOPAL, I., GROVER, G. AND SIDI, M. Real-time packet switching: a performance analysis, *IEEE J.*, 1988, SAC-6, 1576-1586.
2. SASAKI, G. Input buffer requirements for round robin polling systems, *Proc. 1989 Allerton Conf. on Commun., Control and Computing*.
3. CHEN, J. S.-C., GUERIN, R. AND STERN, T. E. *Markov-modulated flow model for the output queues of a packet switch*, IBM Res. Rep. RC 14988 (# 66461) 8/10/89.
4. FRENCH, S. *Sequencing and scheduling: an introduction to the mathematics of the job-shop*, 1982, Ellis Horwood.
5. LIU, C. L. AND LAYLAND, J. W. Scheduling algorithms for multiprogramming in a hard real-time environment, *J. Assoc. Comp. Mach.*, 1973, 20, 46-61.
6. TOBAGI, F. A. Fast packet switch architectures for broadband integrated services digital networks, *Proc. IEEE*, 1990, 78, 133-167.
7. MEISLING, T. Discrete-time queueing theory, *Op. Res.*, 1958, 6, 96-105.

### Thesis Abstract (M.Sc.(Engng))

**Laser patterning and automated loss measurements for integrated optics by Mahadev Gurunath Lad**  
 Research supervisors: A. Selvarajan and H. L. Bhat  
 Department: Electrical Communication Engineering

#### 1. Introduction

Light wave technology has seen rapid advances in the past two decades. Following the same path as electronic ICs developed, various devices and components are being fabricated on a single chip in photonics also. Though the technology is similar, the processes and techniques of obtaining the devices for photonics differ from the electronics

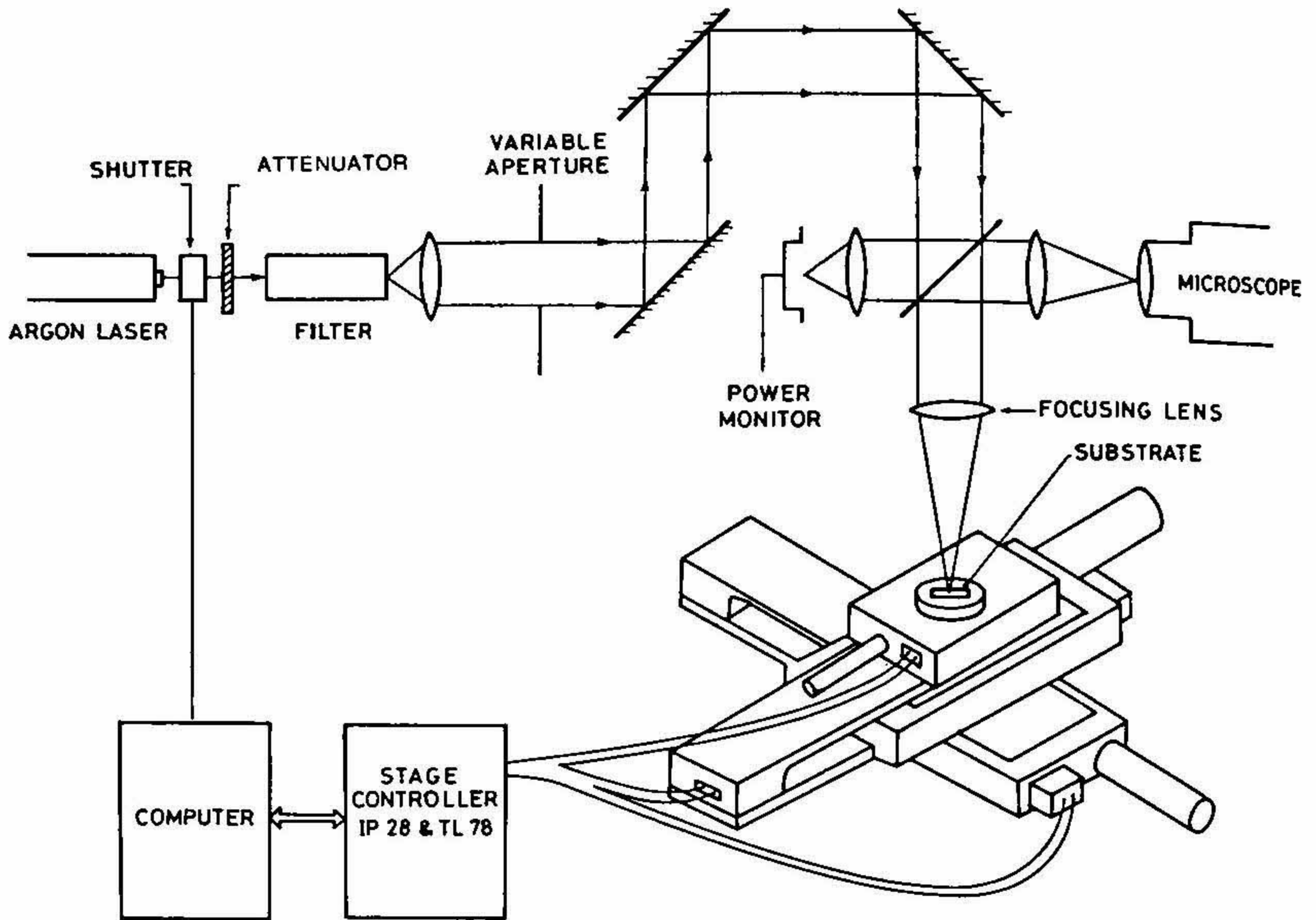


FIG. 1. The schematic diagram of the direct laser writing system.

depending upon the materials. The thesis describes the work done to overcome some of the drawbacks in the conventional methods. Two main aspects—waveguide patterning and waveguide characterization—are addressed in this regard.

## 2. The laser patterning

Integrated optical circuit (OIC) needs lithography as one of the steps in its fabrication. Photolithography is generally adopted to obtain the masks and devices are then processed using these masks. However, because of various drawbacks conventional photolithography is not suitable to obtain the OICs. It is specially so for a research laboratory, where one has to introduce modifications quite often in the designs. Direct laser writing, in which the sharply focussed laser beam is used to draw the desired patterns on the photoresist-coated substrates, proves to be a better method. Such a system has been developed by us. The masks for integrated optical components such as channels, bends and power splitters are obtained using the developed system with good accuracies. The schematic of the system is shown in Fig. 1.

It essentially consist of three parts. An argon laser as the source; the optics consisting of mirrors, lenses, filter and attenuators; and controlling electronics which includes the micropositioner system.

## 3. The automatic loss measurement method

The attenuation coefficient of thin film waveguides is a significant parameter for the evaluation of its usefulness for OICS. Many methods were reported earlier which are either tedious or destructive. Since the brightness of the guided wave streak (*i.e.*, the scattered light intensity) is proportional to the guided light intensity at each point, the measurement of scattered light intensity distribution along the propagation direction of a guided wave enables the determination of propagation loss. Observing the streak through a CCD camera along with a frame grabber helps in the automation of the system. The data obtained can be processed using a computer and the losses can be easily

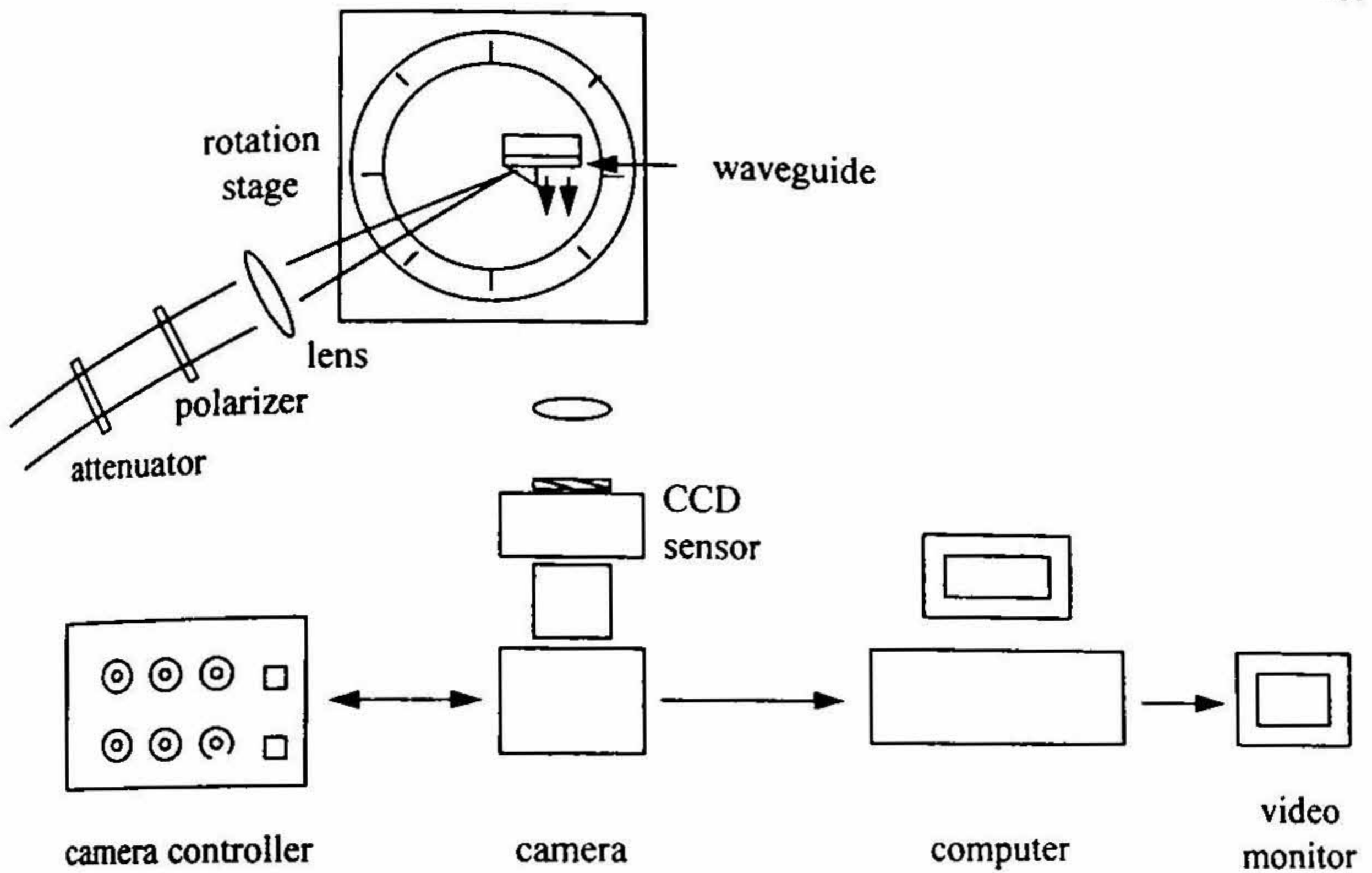


FIG. 2. Schematic of waveguide loss measurement system.

estimated. One such real-time, noncontact type loss-measuring system has been developed as a part of the thesis work. The schematic diagram of the developed system is shown in Fig. 2.

The prism-coupling technique is used to excite the desired mode in the waveguide. The light streak of the guided wave is observed by a CCD camera through a focussing lens. The video signal output from the camera is fed to a digitizer which is incorporated in a personal computer. A video monitor is also connected to the digitizer so that the streak can be seen on the monitor. The computer is programmed to grab the light streak and to process the information to evaluate the propagation loss of the waveguide.

Loss measurements were done on gelatin  $K^+$ - and  $Ag^+$ -ion exchanged, photoresist and Ti-diffused lithium niobate waveguides.

#### 4. Conclusions

The patterns such as parallel waveguides, X, Y splitters and bends of required dimensions are obtained with sufficient accuracy. Hence the developed laser patterning system is quite capable of sufficing the needs of the integrated optics.

Planar waveguides were fabricated using different materials and loss measurements were carried out on them using the loss measurement system developed in our laboratory. Losses ranging from 0.6 to 20 dB/cm were obtained for different materials. From these results, it is clear that this system can be used as a reliable tool to study the propagation losses of integrated optical waveguides.

#### References

1. HARUNA, M., YOSHIDA, S., TODA, H. *Appl. Opt.*, 1987, 26, 4587-4592.  
AND NISHIHARA, H.
2. OKAMURA, U., YOSHINAKA, S. *Appl. Opt.*, 1983, 22, 3892-3894.  
AND YAMAMOTO S.
3. OKAMURA, Y. AND YAMAMOTO, S. *Appl. Opt.*, 1983, 23, 3506-3508.

## Thesis Abstract (M.Sc.(Engng))

### Design of induction heaters by Kamalesh Chatterjee

Research supervisor: V. Ramanarayanan

Department: Electrical Engineering

#### 1. Introduction

Electrical energy may be advantageously used for heating application. The advantages are wide availability of electrical energy, high efficiency, low maintenance and running cost, cleanliness and ease of control. Among the various types of electrical heating, induction heating is widely used in industry for melting, brazing and surface hardening applications. It can also be used for cooking. Advantages over commonly used resistance heaters are safety, better efficiency (long as well as short run) and durability. The limitations are its high cost and suitability for only steel vessels.

The design of induction heating equipment involves the following aspects:

1. Magnetic circuit (the coil to produce the required magnetic field).
2. Electric circuit (the converter to excite the coil to generate the dynamic magnetic field).
3. Control and protection circuits (to control power transfer and to improve reliability).

This work consists of the design of the magnetic circuit, the electric circuit and the control and protection circuits for induction heaters in home application.

#### 2. Magnetic circuit

In kitchen flat-bottom vessels are popular as containers. For heating flat-bottom vessels, a pancake configuration of induction coil is well suited. (Fig. 1).

Calculation of inductance of such a pancake coil is necessary in order to develop design relationships. This has been done from the basic principles of electromagnetism. For each turn, its self and mutual inductance with all other turns are calculated and added together. Total inductance is the sum of all these results.

With reference to Fig. 1, the effective field strength may be increased by providing low reluctance return path at the bottom of the coil as shown in Fig. 2. It is possible to relate, empirically, the predicted results of symmetrical coils to the measured results of asymmetrical coils.

#### 2. Modeling of induction heating loads

Design of the power converter which excites the coil requires knowledge of the electrical behavior of the coil vessel set-up of Fig. 2. A simple circuit model is presented in Fig. 3 where  $R_p$  is the parasitic winding resistance,  $L_m$ , the mutual inductance of the coil and the vessel,  $L_p$ , the leakage inductance of the coil, and  $R_v$ , the resistance representing the loss in the vessel.

It is possible to calculate the coil parameters from simple measurements done on the coil terminals. It has been shown that the important coil parameters are independent of frequency, which has also been experimentally verified.

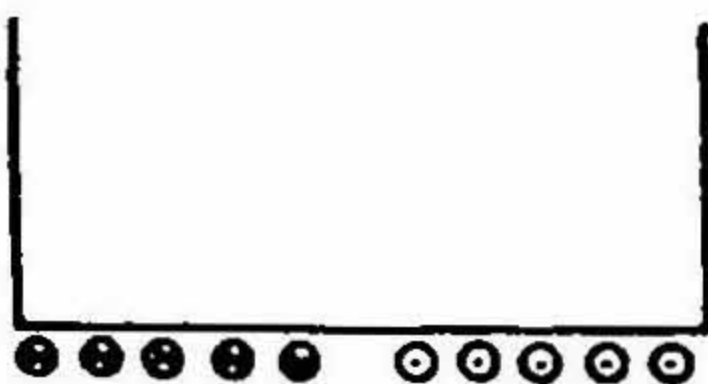


FIG. 1. Pancake coil and flat bottom vessel.

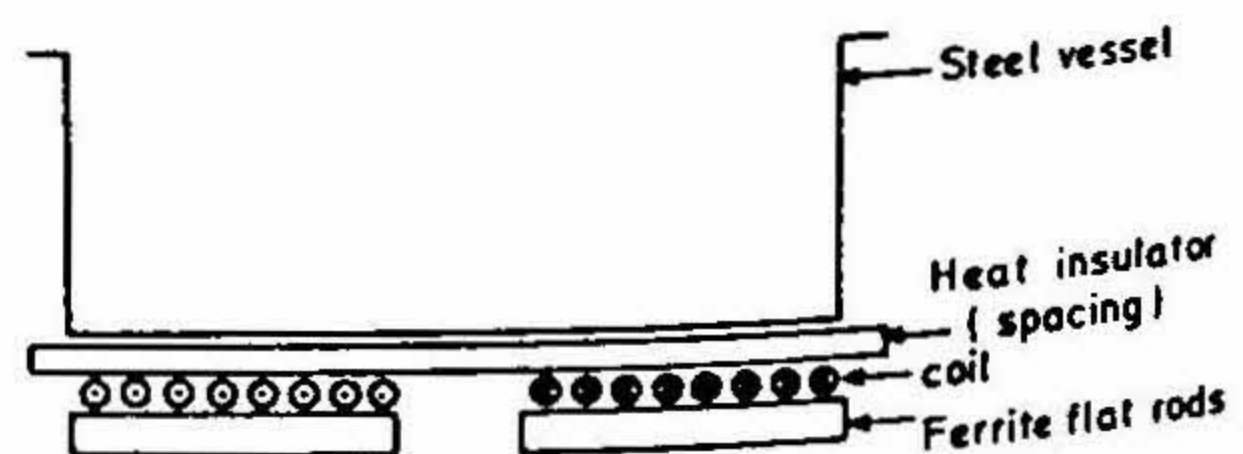


FIG. 2. Pancake coil with a flat bottom vessel. (Actual set-up).

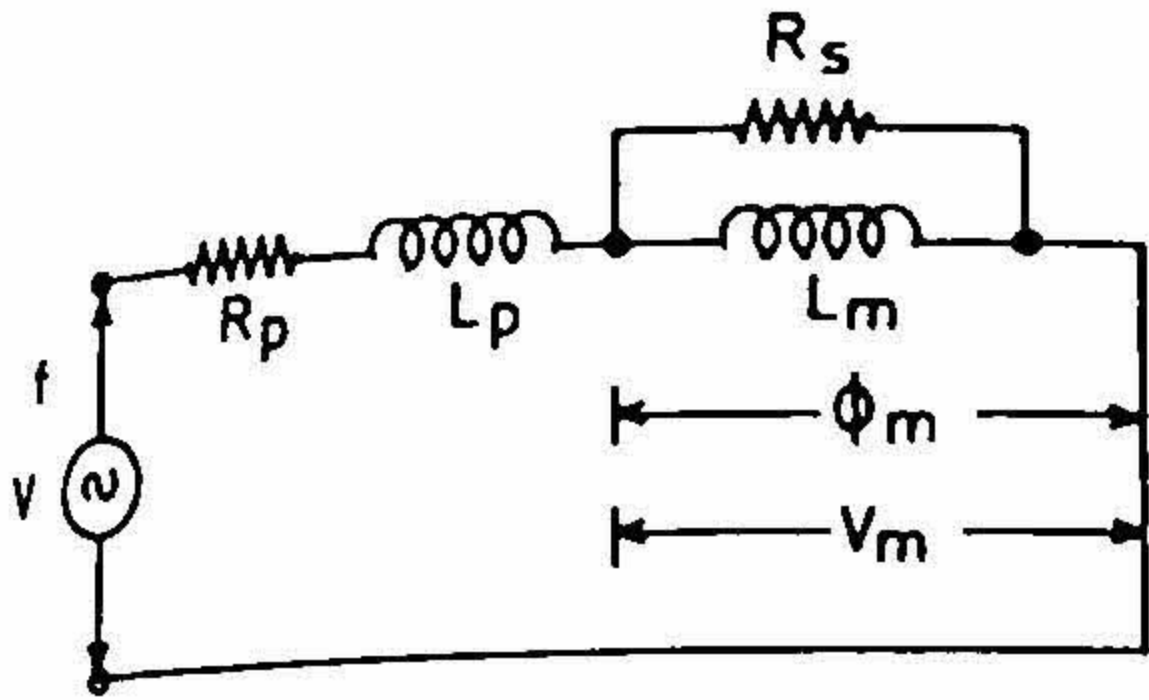


FIG. 3. A simple circuit model.

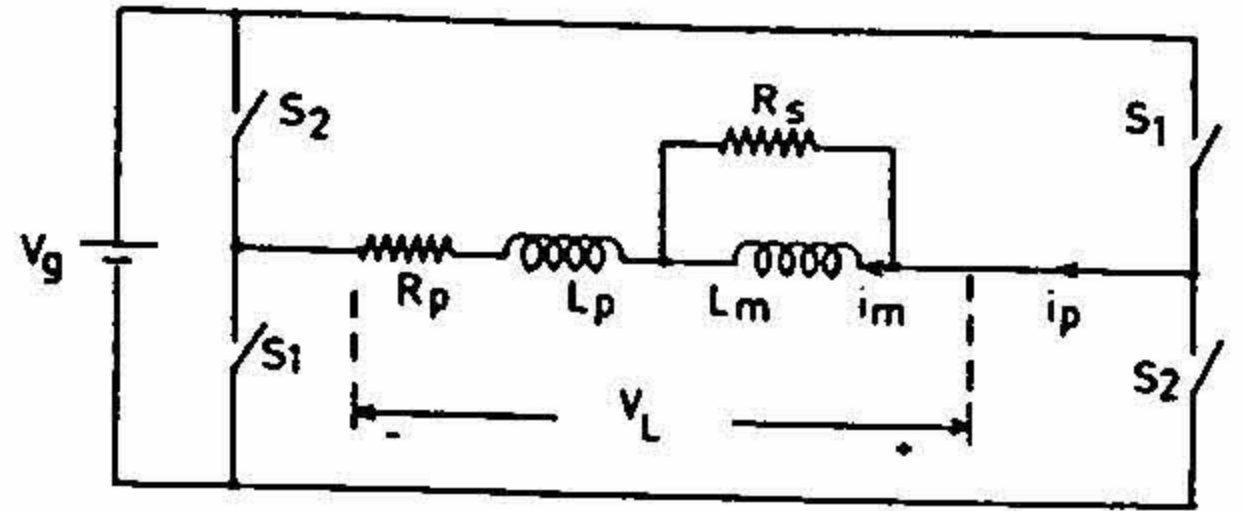


FIG. 4. Full bridge inverter.

Two important parameters useful for the design are the coupling factor  $k [L_m / (L_m + L_p)]$  and the characteristic time constant  $\tau [(L_m + L_p) / R_s]$  of the coil. Measurements on representative coils give likely values of these parameters.

### 3. The power converter

The power converter for exciting the coil mainly consists of an uncontrolled rectifier followed by an inverter. The inverter is the most expensive and important part of the heater. The inverter circuits which are suitable for this application are: 1. Bridge inverter (Fig. 4), 2. Single switch resonant inverter (Fig. 5), 3. Series resonant inverter (Fig. 6).

The defining equations are formulated in per unit system. Such a formulation is helpful for comparison of the performance of different power circuits as well as the design of the same. Performance results are obtained by solving the system equations numerically.

The active switches in the inverter circuits are the most expensive elements. It is desirable that the switches are put to best use. A performance index called switch utilization factor (UFS) is defined as

$$UFS = (P_o \times 100\%) / (V_{sp} I_{sp} n)$$

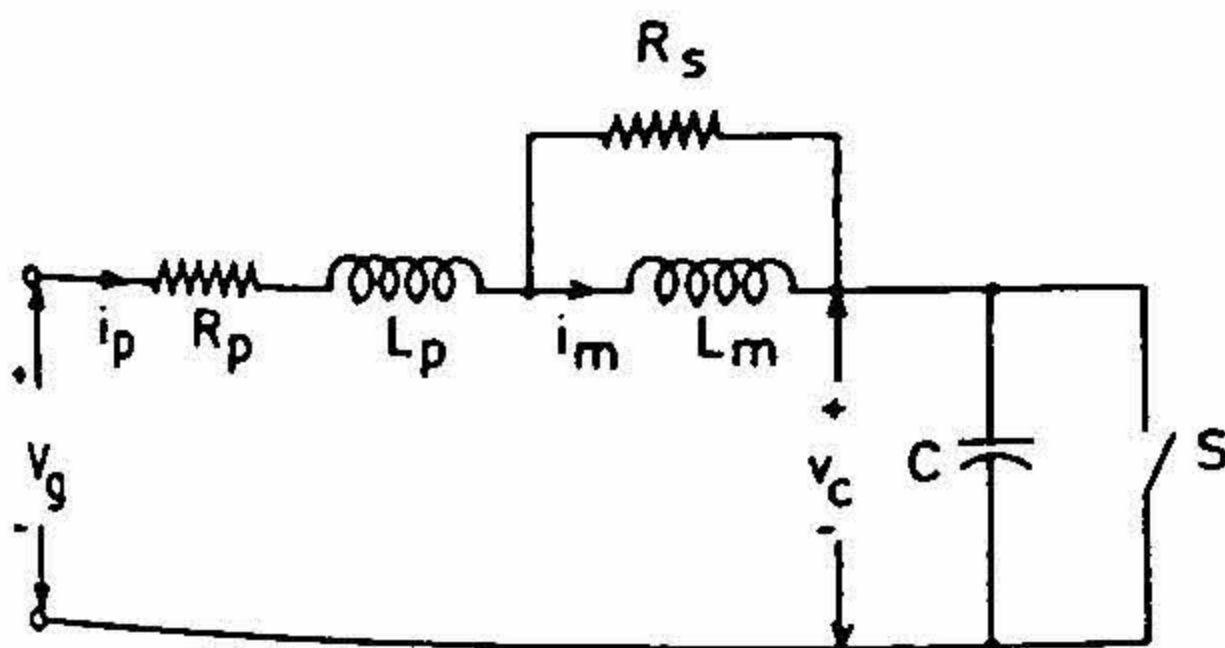


FIG. 5. Single switch voltage-fed resonant inverter.

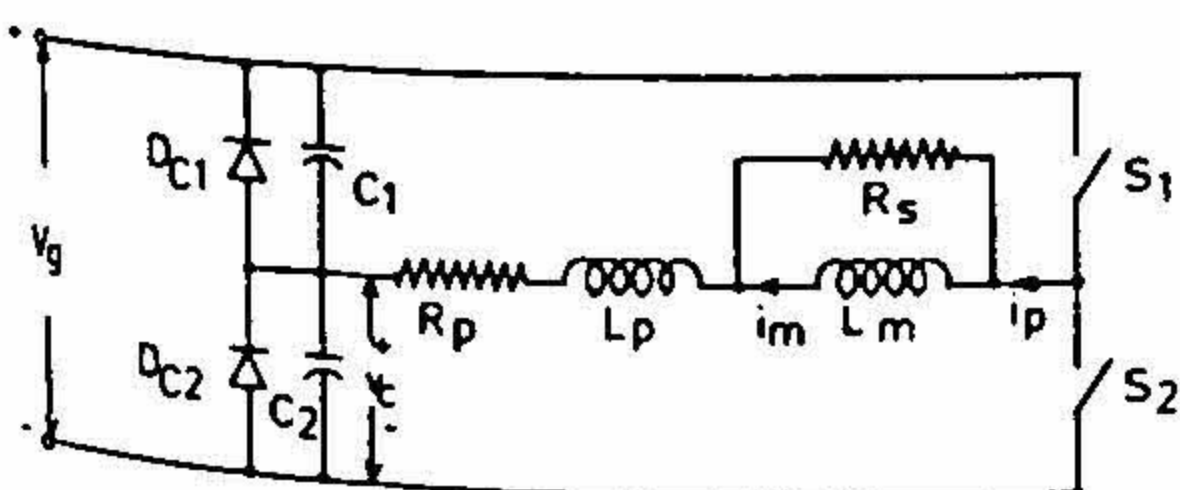


FIG. 6. Voltage clamped series resonant inverter (symmetrical circuit).

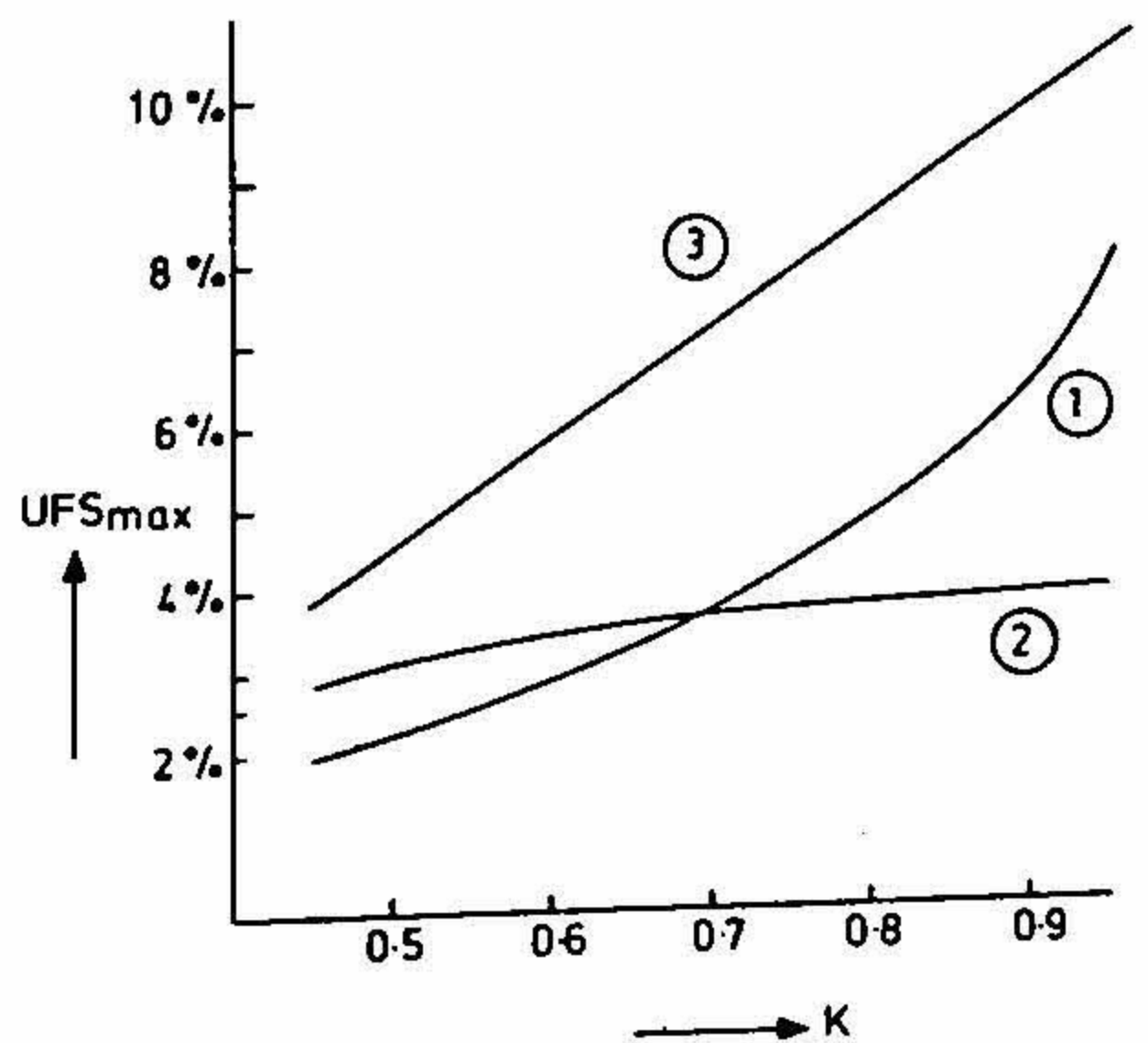


FIG. 7. Switch utilization of different circuits.

where  $P_0$  is the output power,  $V_{sp}$ , the peak voltage across the switch,  $I_{sp}$ , the peak current through the switch and  $n$ , the number of active switches. A higher value of UFS indicates better utilization of the switches.

For each of the circuits a design procedure to realize the operating point where switches are best utilized is presented. Among the circuits studied, the series inverter is found to utilize the power switches best. Figure 7 shows switch utilization factor as a function of the coupling factor for different inverters.

A 110-V, 500-W induction heater is built with a series inverter to verify the design procedure. Its hardware description, control technique and protection feature are given in the thesis.

#### 4. Conclusions

This thesis presents a design procedure for induction heaters. The design has been verified by building an induction heater suitable for kitchen application.

Induction heating is feasible for kitchen applications to heat steel vessels. Its advantages over commonly used resistance heaters are better efficiency (long as well as short run), safety and durability.

#### References

1. OMORI, H. AND IWAI, T. Comparative studies between regenerative and non-regenerative topologies of single ended resonant inverters, *Int. High Frequency Power Conversion Conf.*, 1987, April 21-23, 1987, pp. 357-375, Washington, D.C.
2. RANJITH, K. *Simulation, design and construction of a 100 W induction heater*, ME Project Report, Department of Electrical Engineering, Indian Institute of Science, Bangalore, 1991.
3. RAMESH, S. Fail safe proportional base drive, ME Project Report, Department of Electrical Engineering, Indian Institute of Science, Bangalore, 1991.
4. RANJITH, K. *et al.* Single switch resonant converter for induction heating application, *Proc. Brazilian Power Electronics Conf.*, COBEP'91, Dec. 2-5, 1991.
5. RAMO, S., WHINNERY, J. R. AND VAN DUZER, T. *Fields and waves in communication electronics*, 1985, Wiley.
6. Optimum design of single switch resonant induction heater, *IEEE Int. Symp. on Industrial Electronics*, 25-27 May, 1992, Holiday Inn, Xian, China.